Final Report
May 1, 1997 – April 30, 2000

Laser and Radiofrequency Air Plasma Sources

J. E. Scharer, Principal Investigator
Department of Electrical and Computer Engineering
University of Wisconsin
Madison, WI 53706
AFOSR Grant No. F49620-97-1-0262
April 2000

Abstract

Research on 193 nm laser initiation and rf sustainment of seed gases and air plasmas has been carried out. We have obtained $10^{14}/cm^3$, $T_e = 0.3$ eV laser plasmas of 500 cm^3 volumes using an organic gas which has been seeded (8-60 mTorr) in nitrogen at pressures up to atmospheric conditions. Fast Langmuir probe measurements of density and temperature have been carried out utilizing a special shielded probe and boxcar sampling techniques. Photomultiplier measurements of optical emission have shown increased emission with nitrogen pressure which indicates strong coupling and longer lifetimes ($\tau = 10\mu s$) of the absorbed laser flux to the dominant nitrogen species. We have observed and analyzed a new delayed ionization process of a superexcited seed gas state which interacts with the nitrogen background resulting in longer plasma lifetimes. We have also carried out seed argon measurements of radiofrequency power absorption from 1-100 mTorr yielding densities of $2 \times 10^{13}/cm^3$ and temperatures of 3 eV with 8500 cm^3 volumes in a magnetic field of 1.4 kG. The antenna and plasma loading characteristics have been compared with our MAXEB 2-D simulation model and are in very good agreement. We have since carried out experiments in a nitrogen/argon mix at 1-2 Torr pressures and have achieved plasma densities of $5 \times 10^{12}/cm^3$ at 1 eV with 7000 cm^3 volumes at low 0.03 W/cm^3 radiofrequency power levels. The experimental antenna and matching circuit measurements have been compared to our ANTENA-II simulation code and are in good agreement. We have carried out optical emission measurements on these rf-produced plasmas to determine the lifetime under different gas mix conditions to minimize radiofrequency power requirements. We have also developed an analysis and carried out simulations of highly collisional plasmas created by a radiofrequency source and obtained plasma loading resistances identical to that observed by Eckert and Kelly in atmospheric air at 760 Torr. These models have been used to design and scale our antenna and matching system for our laser initiated seed gas atmospheric air radiofrequency plasma sustainment experiment which has been carried out. We have carried out laser initiation and radiofrequency sustainment in a 5 cm diameter chamber with seed gases and nitrogen at up to 10 Torr pressures. Antenna and matching optimization have provided sustained densities of $10^{12}/cm^3$ which could not be produced without the laser initiation.

1

REPORT DOCUMENTATION PAGE

AFRL-SR-BL-TR-00-

$O\ 178$

1. AGENCY USE ONLY *(Leave blank)*	2. REPORT DATE	3.
		01 May 97 to 30 Apr 00 Final

4. TITLE AND SUBTITLE
Laser and Radiofrequency Plasma Source

5. FUNDING NUMBERS
61102f
2301/EX

6. AUTHOR(S)
Professor Scharer

7. PERFORMING ORGANIZATION NAME(S) AND ADDRESS(ES)
University of Wisconsin
750 University Avenue
Madison WI 53706-1490

8. PERFORMING ORGANIZATION REPORT NUMBER

9. SPONSORING/MONITORING AGENCY NAME(S) AND ADDRESS(ES)
AFOSR/NE
801 North Randolph Street Rm 732
Arlington, VA 22203-1977

10. SPONSORING/MONITORING AGENCY REPORT NUMBER

F49620-97-1-0262

11. SUPPLEMENTARY NOTES

12a. DISTRIBUTION AVAILABILITY STATEMENT
APPROVAL FOR PUBLIC RELEASED; DISTRIBUTION UNLIMITED

12b. DISTRIBUTION CODE

13. ABSTRACT *(Maximum 200 words)*

Our current research is concentrated on the radiofrequency sustainment of the laser-excited air plasmas. We have been able to produce high density plasmas of large volumes and are working on optimization of the seed gas and rf antenna configuration to produce them at high pressures with minimum power requirements. We will also have several papers on this as well as grad students presenting the results at the ICOPS conference.

14. SUBJECT TERMS

15. NUMBER OF PAGES

16. PRICE CODE

17. SECURITY CLASSIFICATION OF REPORT	18. SECURITY CLASSIFICATION OF THIS PAGE	19. SECURITY CLASSIFICATION OF ABSTRACT	20. LIMITATION OF ABSTRACT
UNCLASSIFIED	UNCLASSIFIED	UNCLASSIFIED	UL

1 Introduction

We have made substantial progress in producing seeded air plasmas by both laser initiation and radiofrequency sustainment methods. This work has also resulted in a strong research publication record with five journal publications on the research work [1, 2, 3, 4, 5]. Ding, Scharer and Kelly have carried out new research on laser superexcited seed gas states which reduce recombination rates for the plasma compared to standard methods [5]. Of particular note in this research is the high densities achieved (10^{12-14}/cm^3) and large volumes (500-8500 /cm^3) with absorbed and sustained radiofrequency power densities in the range of 70-100 mW/cm^3 at densities in the 10^{12}/cm^3 range with the use of seed gases in air components. In addition, we have carried out creative fast probe, microwave, and optical diagnostic measurements on these plasmas. We have also developed advanced computer programs which describe the radiofrequency antenna coupling, propagation and heating of the air component plasmas which is useful as a diagnostic to compare with experimental measurements at high pressure. The following sections describe these research results. Lists of students and journal and conference publications are also included.

We have obtained laser-formed plasmas with densities of up to 10^{14}/cm^3 in 32 mTorr of organic gas of 200 cm^3 volumes with initially low, 0.3 eV electron temperatures. We have obtained measurements which suggest that laser-produced superexcited states of the organic gas, tetrakis-dimethyl-amino-ethylene (TMAE), molecule and metastable states caused by the addition of 0.1-760 Torr of nitrogen substantially enhance the lifetime of the plasma emission. The lifetime is found to increase with increasing nitrogen concentration. Figure 1 illustrates the laser plasma facility including the special fast Langmuir probe and microwave scattering diagnostics. We plan to further explore and utilize these processes to reduce power consumption at higher nitrogen and atmospheric air pressures by use of spectroscopic, fast probe, and microwave diagnostics in the future. The spectrometer will allow concentrations of metastable nitrogen and superexcited states of the organic gas to be measured and we will seek methods which maximize these processes which reduce the power to sustain the plasma. These processes are important as a method for reducing power consumption in air plasmas whether laser, radiofrequency or electrode sources are used.

We have also constructed a magnetized radiofrequency plasma facility and obtained efficient, steady-state production of plasma densities of 3×10^{13}/cm^3, $T_e = 3$ eV in volumes of 8500 cm^3 in argon at 5 mTorr by means of 1 kW of 13.56 MHz power. The radiofrequency source has also been utilized to obtain 2×10^{12}/cm^3 densities, $T_e = 3$ eV temperatures at the same power level and 8500 cm^3 volume in 100 mTorr N$_2$ plasmas. We find that the magnetic field configuration and intensity plays an important role in producing efficient, high density plasmas. This work is being published in the Physics of Plasmas [4]. We have carried out further research on rf plasma generation at 2 Torr of a nitrogen-argon mixture and very efficient methods for optimizing antenna coupling and plasma initiation are currently being conducted.

We have also utilized our ANTENA [6] and MAXEB [3] simulation codes to design an improved antenna coupling regime for the radiofrequency formed plasmas and to examine the effects of magnetic fields on the wave penetration and absorption for highly collisional air plasmas. Earlier research on the effects of magnetic field for wave penetration in unbounded collisional plasmas has been carried out by Bozeman [7]. We have examined the effects of the antenna coupled spectra, plasma density, collision frequency, radial profiles and magnetic fields and solved the complete boundary value problem utilizing these codes. We find that magnetic fields do have an important effect on the wave penetration at high collisionality. We find that for plasmas with density $n = 10^{14}$/cm^3 and collision frequency 10^9 Hz, for low magnetic fields of 50 G, the wave is absorbed primarily near the edge and does not penetrate to the core. For 1000 G, the wave penetration to
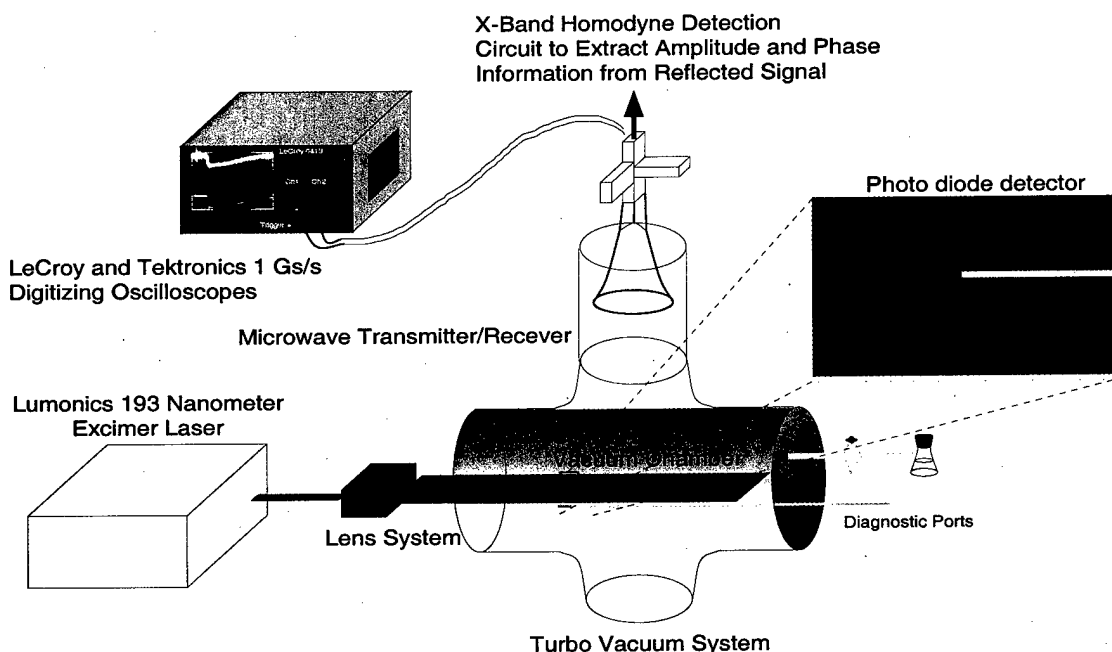
Laser Plasma Experiment

**X-Band Homodyne Detection
Circuit to Extract Amplitude and Phase
Information from Reflected Signal**

Photo diode detector

**LeCroy and Tektronics 1 Gs/s
Digitizing Oscilloscopes**

Microwave Transmitter/Recever

**Lumonics 193 Nanometer
Excimer Laser**

Vacuum Chamber

Diagnostic Ports

Lens System

Turbo Vacuum System

Figure 1: Laser plasma schematic including fast Langmuir probe and microwave diagnostics.

the core is greatly improved and for 2500 G it is optimal. Note that the effect of magnetic fields on wave penetration is even more marked at the peak plasma densities of 10^{13} cm^3. Code runs we have made show even more effective wave penetration, both radially and axially, at this density and high collisionality. We also find that at high collisional values of $\nu = 10^{10}$/s, higher initial plasma densities of 10^{14}/cm^3 and higher frequency operation at 200 MHz also enhances coupling and wave penetration.

The use of our 193 nm excimer laser for initiation of 10^{14}/cm^3 density seed plasmas at higher atmospheric pressures can provide improved initial radiofrequency coupling for sustainment of high density plasmas. The use of radiofrequency waves with the appropriate coupling can enhance the superexcited states of the organic seed gas and the metastable nitrogen which enhance plasma lifetime.

1.1 Laser creation of TMAE plasma in air and its characteristics

The mechanism for TMAE plasma creation is photon absorption. If a photon with sufficient energy is incident on a TMAE molecule, we might expect the TMAE molecule to break into an electron-ion pair. Just such a situation arises when 193 nm VUV (6.4 eV/photon) laser radiation illuminates a chamber filled with TMAE vapor with an ionization potential of 6.1 eV [1]. The cross section for such a reaction is $\sigma = 1.1(\pm 0.3) \times 10^{-17}$ cm^2 [8]. The TMAE molecule is chosen because it has such a low ionization potential and is easily ionized by such laser radiation.

For a TMAE pressure of 32 mTorr, the $1/e$ absorption length of the laser is of the order of 1 m. Microwave reflectivity measurements were carried out on this [2] plasma to observe the properties of the plasma such as collisionality, axial density variation, and plasma decay rates. The results

3

of this study indicate that using a high powered 300 mJ/cm^2) laser is beneficial in creating a high density ($n_e > 10^{14}$/cm^3) seed plasma in air.

### 1.1.1 Estimation of the maximum plasma density

We increased the laser power density to 2 MW/cm^2 and induced the new delayed mechanism of ionization as discussed above, so that we can both increase the initial plasma density and slow down the decay process which is equivalent to reducing the recombination coefficient. Using this new data, we estimate [9] that we obtain peak electron densities of 1.1×10^{14}/cm^3.

1.1.2 Increase in the plasma emission lifetime by addition of 760 Torr of Nitrogen

In the laser experiment, we have found that the addition of up to 760 Torr of nitrogen can slow down the decay of our TMAE plasma optical emission. This phenomenon provides us with a new way to increase TMAE plasma lifetime, and this method is especially useful for TMAE seed plasmas in air. The study of this phenomenon is not only useful for laser produced plasma, but also useful for our radiofrequency method to create plasma in air seeded with TMAE vapor. The experimental results when N$_2$ is introduced into the laser produced TMAE plasma, have been discussed in our AIAA paper [10]. The results show that the higher the N$_2$ concentration, the stronger the effect. N$_2$ plays an important role in slowing down the plasma emission decay process.

The plasma and chemical processes are quite complicated, but we assert that the following two mechanisms are most dominant for this phenomenon.

(1) There is an additional reaction when N$_2$ is added

$$TMAE^{**} + N_2(X) \rightleftharpoons N_2^*(A) + TMAE(X) \tag{1}$$
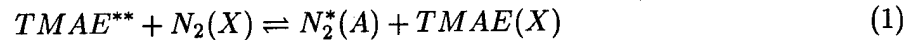
where $TMAE^{**}$ is the TMAE molecule in the superexcited state which we described above, X stands for the ground state, and $N_2^*(A)$ is a metastable state of nitrogen. The 6.4 eV energy of TMAE** provided by the laser is precisely in the band of metastable state of $N_2(A^3\Sigma_u^+)$, so that the transfer rates in Eq. (1) are expected to be very high. Since the metastable state N$_2$(A) has a long-lifetime (1.9 s), its density decay is much slower than that of both TMAE** and TMAE$^+$. So the reverse reaction of Eq. (1) keeps the superexcited TMAE** density from rapidly decaying, and the auto-ionization of the superexcited TMAE** state can slow down the plasma density decay.

$$TMAE^{**} \longrightarrow TMAE^+ + e \tag{2}$$

(2) Another possible mechanism is the Penning ionization

$$N_2^*(A) + TMAE(X) \longrightarrow TMAE^+ + e + N_2(X) \tag{3}$$
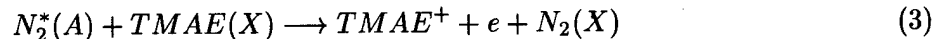
Since the energy of $N_2^*(A)$ exceeds the ionization potential of TMAE, this reaction is quite likely occur. When the molecular densities of both TMAE and $N_2^*(A)$ are high, this reaction is believed to be very fast. We plan to further investigate and exploit this process to provide reduced power consumption for high density air plasmas in the proposed research.

2 Laser Produced TMAE Plasma in Nitrogen

2.1 Lab apparatus

A schematic experimental arrangement is illustrated in Fig. 2. A laboratory plasma is created in a 50-cm-long by 15.2-cm-diameter cylindrical glass chamber, which is pumped to a base pressure

of 5×10^{-7} Torr by a diffusion pump. A Suprasil window which is transparent down to 180 nm wavelengths is mounted on the laser entrance end of the vacuum chamber. On the opposite side of the chamber, a Langmuir probe and a flow feed to introduce the TMAE vapor are inserted through feed-throughs to the vacuum chamber.

A Lumonics PM842 excimer laser runs in an ArF mode and produces 193 nm wavelength radiation. The half-width of the laser pulse is 20 ns. The shape of laser output cross section initially is a rectangle of 3 cm × 1.3 cm. It can be changed simply by a two-lens system. In this experiment, the laser first passes through a beam splitter, and the output cross section is changed to 2.4 cm × 1.3 cm. Then the laser passes through a two-lens system, and its output cross section is changed to 2.4 cm × 3.2 cm. The laser beam is quite uniform, $\Delta I/I \le 10\%$ as measured by an apertured photodiode. A calorimeter is used to accurately measure the intensity of the laser beam.

2.2 Diagnostic for TMAE and nitrogen mixture plasma

The electron density can be measured from Langmuir probe electron saturation currents which are independent of the ion species and mixture. However, a simple probe structure is not suitable for this measurement because:

1. The detection system must have a very good high frequency response. We have developed a fast response detection system which can measure Langmuir probe current-voltage characteristic curve at a certain delay time after the laser pulse. The frequency response is measured as follows: A signal generator replaces the probe tip. The input signal is compared with output signal from the complete probe circuit and data acquisition system. The wave signals are varied from 200 MHz to 20 kHz. The output signal amplitudes are slightly reduced compared to the input, and the relative errors from 20 kHz to 2 MHz is below 0.5%, and that for 2 MHz to 20 MHz is below 1%.

2. For an organic gas plasma, probe contamination by condensates can substantially disturb the measurements. An indirect heating technique is applied to the probe to ensure that its surface is very clean.

3. For a rapidly pulsed plasma, the noise from the plasma as well as from the laser discharge can severely perturb the probe measurement, and the isolating and shielding layers around the Langmuir probe may not be perfect. One way to check the noise perturbation is by means of a dummy probe method. The dummy probe is an identical probe to the measurement probe, except that it is not exposed to the plasma. In this experiment, the signal from the dummy probe is always smaller than 0.1% of the electron saturation current obtained from the measurement probe.

   The new probe structure is shown in Fig. 3. The Langmuir probe current-voltage characteristic curve is measured by a sampling technique with a boxcar integrator. A typical I-V characteristic is shown in Fig. 4.

Collisionless Langmuir probe theory is valid for the 200 mTorr nitrogen case, because the electron mean-free-path (3 mm) is much larger than either the probe size (0.25mm) or Debye length (0.01 mm scale).

In order to diagnose the plasma in high pressure conditions, a photo-multiplier tube is utilized to collect the plasma emission light from the perpendicular direction to the laser beam.
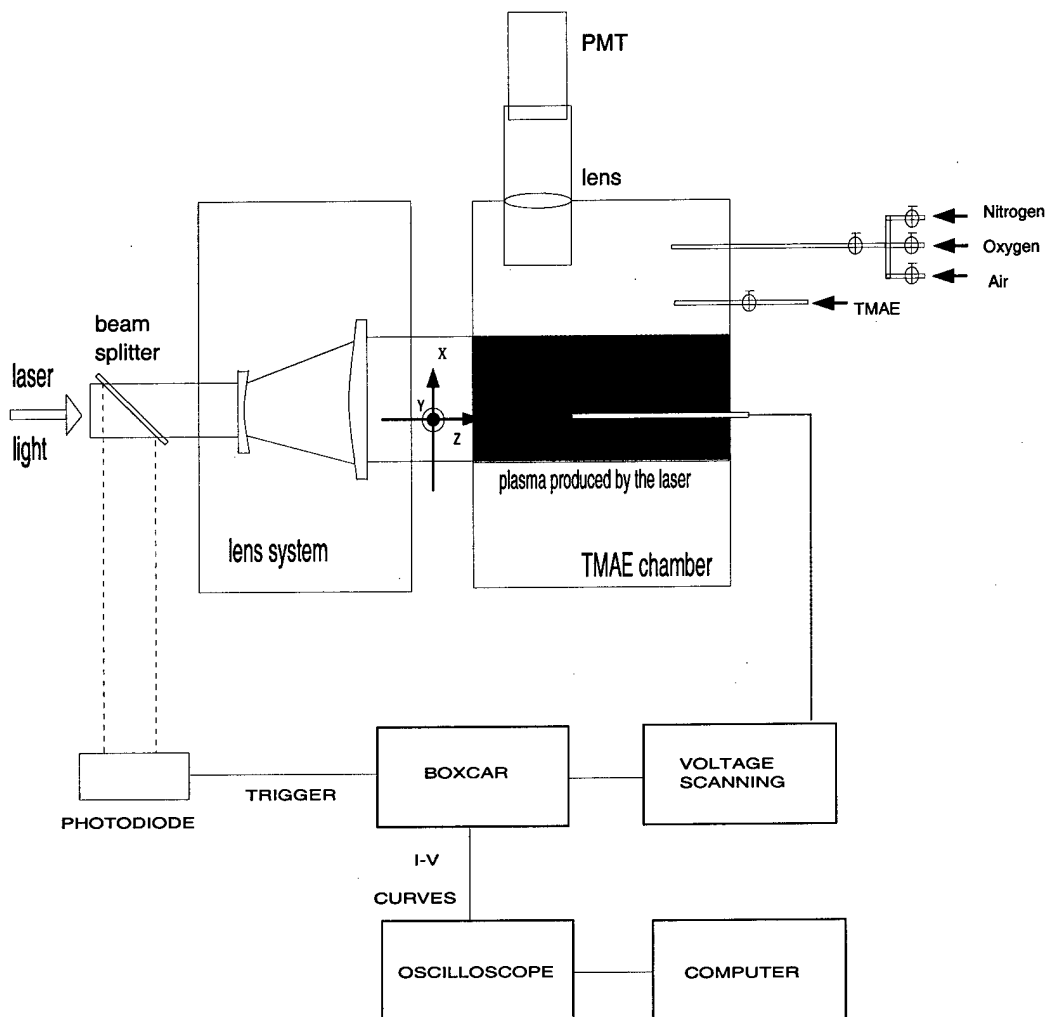
Figure 2: Schematic of the experimental arrangement and Langmuir probe characteristic measurements.
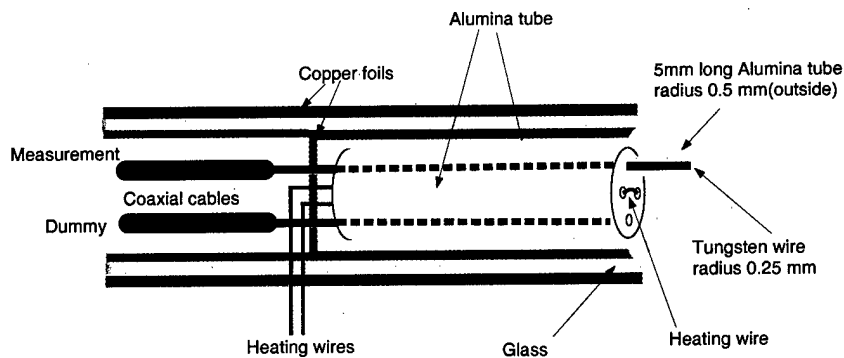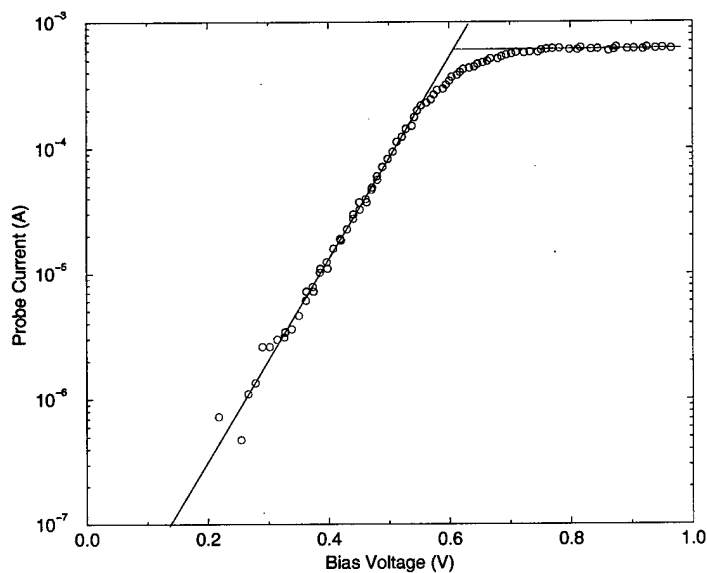
Figure 3: Langmuir probe structure.

Figure 4: Typical I-V characteristic from Langmuir probe measurement, taken under 16 mTorr TMAE and 200 mTorr nitrogen pressure, laser fluence is 4 mJ/cm^2 and the delay time after the laser pulse is 1500 ns.
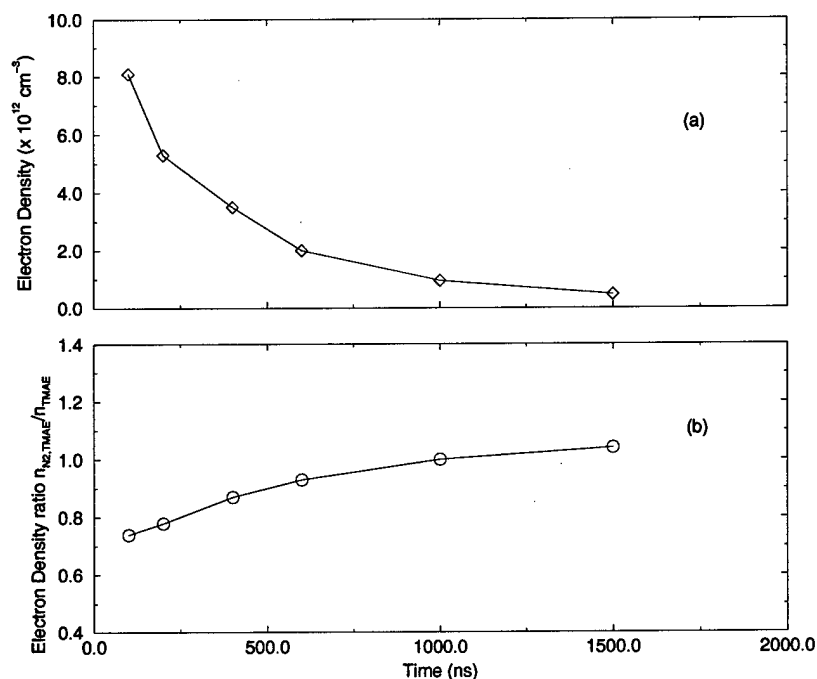
Figure 5: (a) Electron density for nitrogen-TMAE mixture plasma with 200 mTorr nitrogen, 16 mTorr TMAE and 4 mJ/cm^2 laser influence. (b) the density ratios between nitrogen-TMAE plasma and pure TMAE plasma.

2.3 TMAE plasma in nitrogen

The time dependence of the electron densities of TMAE-nitrogen mixture plasma case is shown in Fig. 5. The density ratio between the mixture and the pure TMAE plasma are shown in Fig. 5(b). The electron temperature decay for the two cases are almost identical, which are shown in Fig. 6. At early times (hundreds of nanoseconds), the electron density with nitrogen mixture is lower than those with a pure TMAE plasma. However, their density ratios increase with time in Fig. 5(b).

The plasma emission measurement is shown in the Fig. 7. When 0.5 Torr nitrogen is mixed with TMAE in the chamber, the emission during the initial microsecond becomes smaller than that of the pure TMAE plasma. But as more and more nitrogen is added, the emission becomes stronger and stronger.

Many physical processes influence the results [9], and here we discuss some of the possibilities.

1. For the pure TMAE plasma, we have found that two processes are dominant in the decay process, electron-ion recombination and delayed ionization, but other processes, such as three-body recombination and diffusion processes are not important at low gas pressure and on microsecond time scales. Delayed ionization is an ionization process ntial (I.P.), they do not necessarily promptly ionize, especially for a large molecule [11], such as TMAE. When the TMAE molecule is excited by the laser, the total energy (electronic + vibrational + rotational) can exceed the first ionization potential, but the electronic component alone is insufficient for ionization. Such an excited state is called a super-excited state [12]. Such phenomenon has been found in many organic molecules. TMAE can occupy a super-excited state, then undergo ionization or dissociation processes at later times. This is the delayed ionization process, which can slow down the TMAE plasma density decay [13].
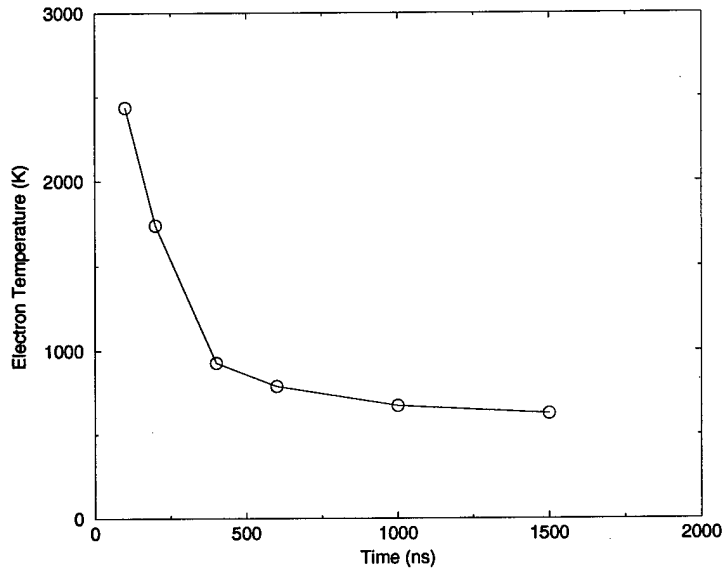
8

Figure 6: Electron temperature variation with time, taken with 16 mTorr TMAE, 200 mTorr nitrogen and 4 mJ/cm^2 laser influence.

2. For the nitrogen-TMAE mixture plasma, delayed ionization through the super-excited state can also be important. Since the energy of the super-excited TMAE** is exactly in the band of metastable state of $N_2(A^3\Sigma_u^+)$, the energy transfer rates between them are expected to be very high. The delayed ionization process is dependent on the super-excited TMAE** which could be influenced by nitrogen. For early times (hundreds of ns), delayed ionization is weakened because many TMAE** molecules transfer energy to $N_2(A^3\Sigma_u^+)$ rather than undergo the delayed ionization process. However, the metastable $N_2(A^3\Sigma_u^+)$ density can increase (the metastable state $N_2(A)$ has a long lifetime (1.9 s), so on a microsecond time scale, $N_2(A)$ density does not decay due to its natural lifetime. At later times, the energy transfer from $N_2(A^3\Sigma_u^+)$ to TMAE** should increase, and Penning ionization between $N_2(A^3\Sigma_u^+)$ and TMAE could occur. Thus, delayed ionization might be enhanced by nitrogen at later times. This is a possible interpretation for Fig. 5(b) which shows that the density ratios increase with time.

3. Assume that in a reaction, part At later times, of the TMAE$^+$ ion is changed to another ion, which has a smaller recombination rate, so that the plasma density decay is reduced. If this process is enhanced by nitrogen, then the nitrogen helps to reduce the plasma density decay. This is an alternative interpretation of Fig. 5(b).

4. In Fig. 7, when 0.5 Torr nitrogen is added, the emission measurement qualitatively agrees with the Langmuir probe measurement, where the nitrogen TMAE mixture plasma has a lower density than the pure TMAE plasma at the initial 1 microsecond. When more and more nitrogen is added to 500 Torr, the emission is stronger and stronger even for the first initial 100 ns. We believe that the mechanisms discussed above are the reasons for these experimental phenomenon. When the nitrogen pressure becomes higher and higher, which means that the mechanisms discussed above become faster and faster, and become more and more important

9

Total Optical Emission Intensity from the Plasma
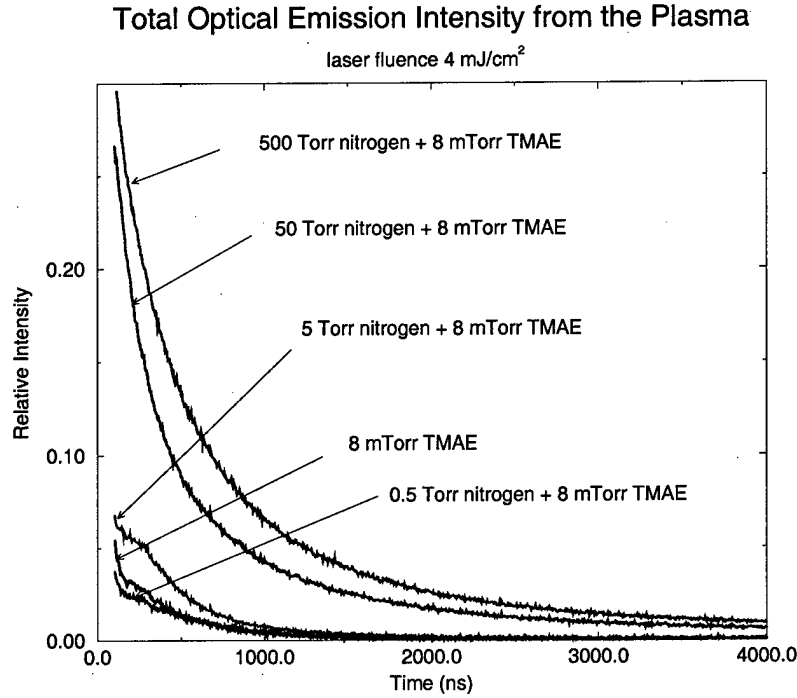
laser fluence 4 mJ/cm^2

Figure 7: Total emission Intensity from laser produced TMAE plasma seeded in nitrogen.

at the earlier times. So where the nitrogen pressure increases, the nitrogen-TMAE plasma is more dense.

2.4 Observation of Delayed Ionization in Laser Formed Plasma

A large volume (hundreds of cm^3) plasma is created by a 193 nm laser ionizing an organic vapor, tetrakis (dimethyl-amino) ethylene (TMAE). The plasma is characterized as high electron density (10^{13} - 10^{12}/cm^3) and low electron temperature ($\sim$ 0.1 eV). To investigate the plasma decay processes, a fast Langmuir probe technique is developed, including a detailed considerations of probe structure, probe surface cleaning, shielding, frequency response of the detection system, physical processes in probe measurement, dummy probe corrections as well as noise analysis. The mechanisms for the plasma decay are studied and a delayed ionization after the laser pulse is found to be important. This mechanism is also supported by optical emission measurements that nitrogen enhances the delayed emission from TMAE plasma. A model combining electron-ion recombination and delayed ionization is utilized together with experimental results to order the terms and calculate the relaxation times for delayed ionization. The relaxation times are longer for lower TMAE pressures and lower electron densities.

2.4.1 Analysis of plasma decay processes

For a source-free plasma, the density decay process is usually described as

$$\frac{dn_e}{dt} = -D \nabla^2 n_e - \alpha_{eff} n_e^2 - \nu_a n_e \tag{4}$$

where D is plasma diffusion coefficient, α_{eff} is the effective recombination coefficient, and ν_a is the electron attachment rate.

Electron attachment

Since TMAE molecule is a strong electron donor rather than an electron acceptor, the rate of electron attachment to TMAE should be small. Since the electron mobility in liquid TMAE is very large [14], this implies that the electron attachment rate to the TMAE molecule should be small. In this experiment, Langmuir probe measurements can determine if negative ions are present. Holmes et al. [15] has given a formula to calculate the negative ion density.

$$\frac{J_{e,sat}}{J_{i,sat}} = \frac{1}{0.6}(1 - \frac{n_-}{n_+})\sqrt{\frac{M_i}{2\pi m_e}} \tag{5}$$

where M_i is the positive ion mass, m_e is the electron mass; n_- and n_+ are the negative and positive ion density respectively; $J_{e,sat}$ and $J_{i,sat}$ are electron and ion saturation current density. If negative ion formation is important, n_-/n_+ should increase with time due to rapidly decaying in n_+ and increasing in n_- from zero, so that the electron and ion saturation current density ratio $J_{e,sat}/J_{i,sat}$ should decrease with time. However, no decreasing trend of ratio $J_{e,sat}/J_{i,sat}$ with time can be found within 10% over 2 μs. Thus, the electron attachment effect must be very small for our experimental conditions over the initial 2 μs.

Electron-ion recombination

With the neglect of both diffusion and electron attachment processes, which are small in the experiment, Eq. (4) becomes

$$\frac{dn_e}{dt} = -\alpha_{eff}n_e^2. \tag{6}$$

The solution to this equation is

$$\frac{1}{n_1} = \frac{1}{n_0} + \int_{t_0}^{t_1} \alpha_{eff}\, dt. \tag{7}$$

where n_0 and n_1 are the electron densities at times t_0 and t_1 respectively. The effective α_{eff} in this manuscript are approximately calculated from the corresponding electron densities at two successive measurement times.

$$\alpha_{eff} = (\frac{1}{n_1} - \frac{1}{n_0})/(t_1 - t_0). \tag{8}$$

We plot α_{eff} versus time for different experimental conditions in Fig. 8. The results show that α_{eff} is not constant with time, but increasing. The higher the TMAE pressure, the more rapid the increase in α_{eff} with time.

Another result is that the change in α_{eff} is only weakly dependent on the change in electron temperature. One can write the first order relationship as

$$| \Delta\alpha_{eff} |_{due\ to\ Te\ effect} = | \frac{\partial\alpha_{eff}}{\partial T_e} | \cdot | \Delta T_e | \tag{9}$$
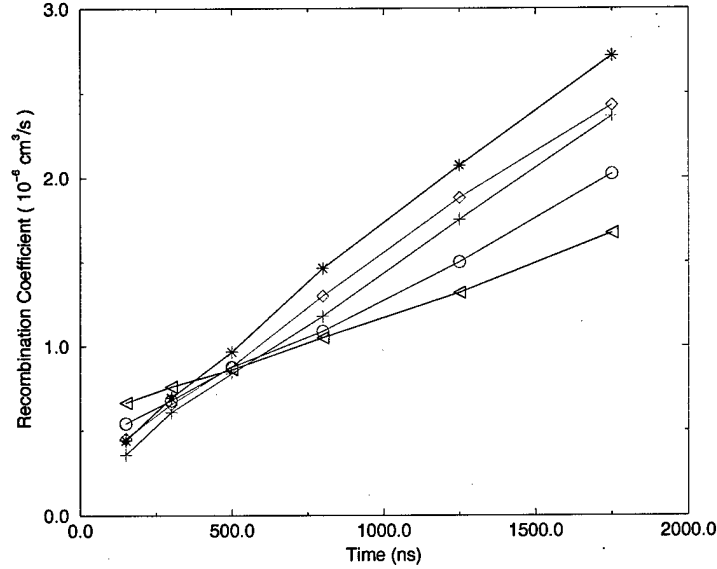
11

Figure 8: Effective electron-ion recombination coefficient vs. time under conditions of 4 mJ/cm^2 laser fluence with TMAE pressure of ($\star$) 16 mTorr, ($\diamond$) 8 mTorr, ($\circ$) 4 mTorr, ($\lhd$) 2 mTorr and under 8 mJ/cm^2 laser fluence with TMAE pressure of ($+$) 8 mTorr.

If the electron temperature T_e effect were important in the change in α_{eff}, the larger $|\Delta T_e|$ should cause the larger $|\Delta\alpha_{eff}|$, but the experimental results in Fig. 9 shows the opposite. First, from t=100 ns to t= 2000 ns, $|\Delta T_e|$ for the 2 mTorr TMAE case is larger than that of 16 mTorr case, but $|\Delta\alpha_{eff}|$ in the 2 mTorr case is smaller than that of 16 mTorr case. Second, for the 16 mTorr TMAE pressure case, T_e is almost constant in time (0.6 $\mu s < t < 2$ μs), but the α_{eff} is approximately tripled. These results show that the change in α_{eff} is only weakly dependent on the change in electron temperature. This agrees with a general rule [16] that for a larger molecular ion, α_{eff} is less electron temperature dependent, e.g. $H_3O^+(H_2O)_2$ and $NH_4^+(NH_3)_2$ plasmas [17, 18] which are almost independent of T_e.

The experimental results can not be interpreted by the three-body recombination and muti-ion species effects:

(1) The process of three-body recombination with the electron as the third body (ion + e +e): This process causes α_{eff} to decrease as the electron density decays. This is contrary to the observation that the α_{eff} increases as the electron density decays.

(2) The process of three-body recombination with the TMAE molecule as the third body (ion + e + TMAE): The TMAE density is constant with time, so this process can not interpret the increase of α_{eff} with time. In addition, to our knowledge, there are no reports of such a three-body process being important in the mTorr scale range.

(3) The multi-ion species effect: This effect must cause α_{eff} to decrease with time. If two components are assumed, the component with a larger α_j decays more rapidly, so the proportion of the component with the larger α_j must decrease with time. As a result, the global α_{eff} must decrease with time. This is in conflict with the experimental results of α_{eff} increasing with time. In addition, the ratios $J_{i,sat}/J_{e,sat}$ from the Langmuir probe measurement are constant within the
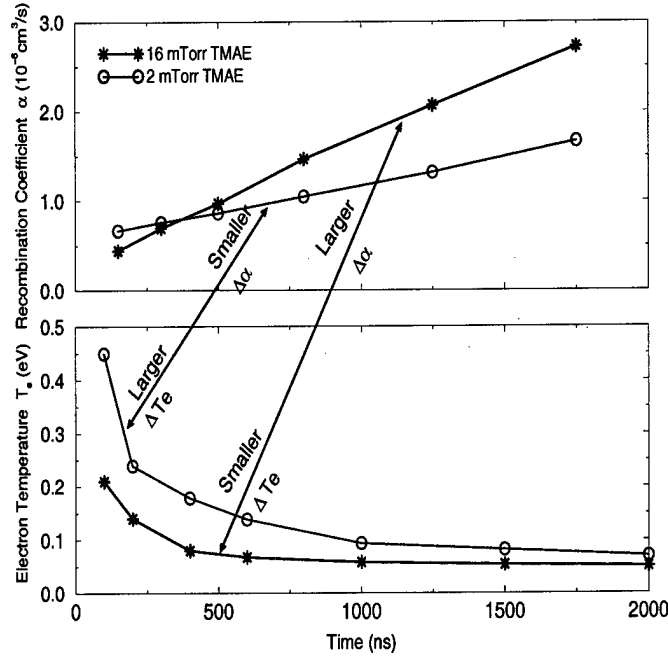
12

Figure 9: Comparison of the variation of α_{eff} and T_e with time under conditions of 4 mJ/cm^2 laser fluence with TMAE pressure of 2 and 16 mTorr.
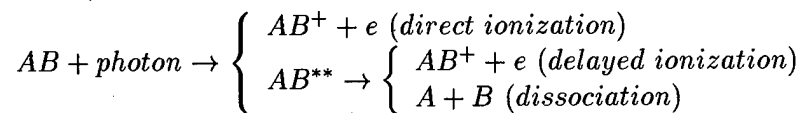
experimental error 10%, which implies that over the initial 2 μs, the ion species doesn't change.

Thus, the experimental observations can not be interpreted by the factors discussed above. This implies that another physical process is important in the decay process of the laser-produced TMAE plasma.

2.4.2 Delayed ionization

Photons absorbed by TMAE molecules may not contribute to direct ionization. When the TMAE molecule is excited by the laser photon (6.4 eV), the total energy (electronic + vibrational + rotational) exceeds the first ionization potential (5.4 eV for TMAE), but some of those molecules are still neutral. Such an excited state is called a super-excited state [19]. This phenomenon has been found in many molecules, including TMAE [20]. For some of them, the lifetime can be hundreds of ns, even tens of μs, and the most prominent example is C_{60} [21, 22]. There are also many reports for other molecules such as benzene [23, 24, 25, 26], benzene clusters [27, 28], benzene-noble gas dimers [29], naphthalene [30], azulene [31], triethylamine [32], ketene [33], Nb, Ta and W clusters [34, 35], C_{70} [21, 36], fullerenes C_n(n<96) [37], etc. There are many theoretical articles too [38, 39]. The experiments and theories are summarized in review articles [40, 41, 42, 43].

When a molecule is excited by a photon with energy higher than its ionization potentials (I.P.), it does not necessarily promptly ionize, particularly for a large molecule [44], the physical processes are illustrated as follows [42, 19, 45]:

$$AB + photon \rightarrow \begin{cases} AB^+ + e \ (direct\ ionization) \\ AB^{**} \rightarrow \begin{cases} AB^+ + e \ (delayed\ ionization) \\ A + B \ (dissociation) \end{cases} \end{cases}$$

where AB^{**} represents molecule AB in a super-excited state.

13

The analysis suggests that a delayed ionization could occur in 193 nm laser photo-ionization of TMAE. There are several arguments to support this interpretation.

First, the delayed ionization mechanism can interpret the "unexplained" experimental observations. (1) The delayed ionization decays rapidly with time, so it becomes less important during later times. This causes α_{eff} to increase with time. (2) As the TMAE pressure increases, due to the collisional reaction TMAE + TMAE**, TMAE** decays more rapidly, so that the delayed ionization process is reduced. This is the reason that the plasma of 16 mTorr TMAE case decays more rapidly than that of 2 mTorr TMAE case.

Second, the delayed optical emission experiments strongly support the delayed ionization interpretation, which will be presented in the next section.

Third, there are many reports on delayed ionization phenomenon in laser ionization of large molecules.

Fourth, TMAE super-excited phenomenon has been reported [20] when excited from 185 nm to 196 nm, although the relaxation time of the delayed ionization is not measured. According to this report, when TMAE is excited by a 193 nm laser, superexcited TMAE** can be created.

In sum, the mechanisms of the laser-produced TMAE plasma decay processes are studied, compared with the experimental measurements, and a delayed ionization process is indicated.

2.4.3 Optical Emission Measurement

A spectrometer at a right angle to the laser beam is utilized to collect the plasma emission. The temporal emission intensity at 480 nm with a 4 nm resolution is shown in Fig. 10. The first peak is primarily a response to laser induced fluorescence (LIF). For later times, such as t > 100 ns, the LIF emission is greatly reduced. Interesting results occur when 5 Torr, 50 Torr and 760 Torr of nitrogen are added to 8 mTorr of TMAE. The emission spectra intensity for 300 ns < t < 1300 ns is increased with increasing nitrogen pressure, as shown in Fig. 11. The relative spectra are very similar for all cases, which implies that the majority species has not changed during this period. The peak of 480 nm has been reported as an emission for a TMAE Rydberg state (R1) which has 20 ns radiative lifetime [46, 47]. Since nitrogen doesn't react with TMAE at the ground state [48], and since nitrogen does not absorb the 193 nm photon, the enhancement of the delayed emission intensity suggests that there should be an energy-storage mechanism during the laser shot, and the energy is released during the delayed processes. The process of the energy-storage should involve a long-lifetime (hundred of nanosecond time scale) and highly excited species (above the first TMAE Rydberg state energy). This species is the source for the enhanced delayed emission.

In sum, the results of the enhancement of the delayed emission from TMAE plasma by the nitrogen suggest that a long-lifetime (hundred of nanosecond time scale) highly-excited state (above the first TMAE Rydberg state energy) is important in the TMAE plasma, which could be a source for the delayed ionization. This result supports the delayed ionization mechanism.

2.5 Model

With the neglect of both diffusion and electron attachment processes, which are small in the experiment, the electron density decay is given by

$$dn_e/dt = (-\alpha_{eff})n_e^2. \tag{10}$$

It is challenging to estimate the relaxation time of the delayed ionization process due to many physical and chemical processes involved. However, the laser-produced TMAE plasma has some
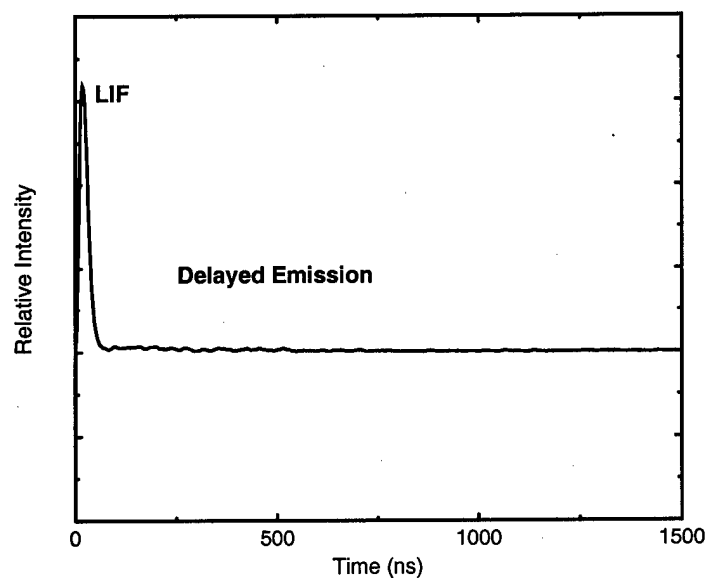
14

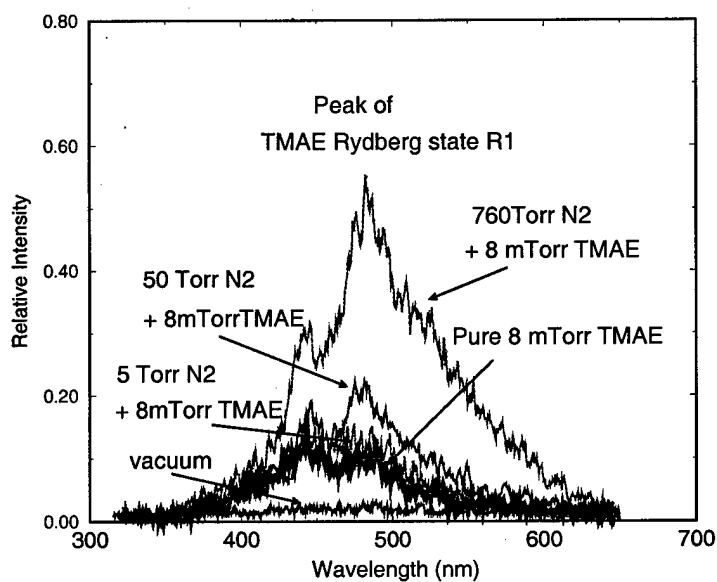Figure 10: The emission temporal profile from laser produced TMAE plasma measured at 480 nm.

Figure 11: Nitrogen effect on delayed emission from the laser produced TMAE plasma emission spectra, measured at time window of 300 ns < t < 1300 ns after the laser pulse.

excellent properties which reduce the number of those processes. In this experiment, diffusion and electron attachment processes are negligible. The other three processes (three-body recombination with either electron or neutral as the third body, electron temperature effect, and multi-ion species processes) have been discussed and shown to be inadequate for interpreting the experimental results. Therefore it is reasonable to assume that the change in the electron density is primarily due to the processes of electron-ion recombination and delayed ionization. So the time derivative of electron density is governed by

$$\frac{dn_e}{dt} = -\alpha n_e^2 + D(t) \tag{11}$$

where n_e is the electron density, α is electron-ion recombination rates, and $D(t)$ is the delayed ionization rate.

Substituting Eq. (10) into Eq. (11),

$$dn_e/dt = (\alpha - \alpha_{eff})n_e^2. \tag{12}$$

The physical meaning of $\alpha - \alpha_{eff}$ is the change in the effective recombination coefficient due to the delayed ionization process.

The relaxation time, τ, of the delayed ionization can be defined as

$$\tau = \frac{-1}{\frac{d\,lnD(t)}{dt}}. \tag{13}$$

We substitute Eq. (10) into Eq. (12), and neglect $d\,ln(\alpha - \alpha_{eff})/dt$. Thus the relaxation time τ can be calculated approximately as

$$\tau = \frac{-1}{\frac{d\,ln[(\alpha - \alpha_{eff})n_e^2]}{dt}} = \frac{-1}{\frac{d\,ln(\alpha - \alpha_{eff})}{dt} + \frac{d\,ln(n_e^2)}{dt}} \approx \frac{-1}{\frac{d\,ln(n_e^2)}{dt}}. \tag{14}$$

Here the approximation is valid if

$$\left| \frac{d\,ln(\alpha - \alpha_{eff})}{dt} \right| \ll \left| \frac{d\,ln(n_e^2)}{dt} \right|. \tag{15}$$

Since $\left| \dfrac{d\,ln(\alpha - \alpha_{eff})}{dt} \right| = \left| \dfrac{\frac{d\alpha}{dt} - \frac{d\alpha_{eff}}{dt}}{(\alpha - \alpha_{eff})} \right|$, the validation of Eq. (15) needs two conditions, namely

$$\left| \frac{d\alpha}{dt} \right| \ll \left| \frac{d\alpha_{eff}}{dt} \right| \tag{16}$$

and

$$\left| \frac{\frac{d\alpha_{eff}}{dt}}{(\alpha - \alpha_{eff})} \right| \ll \left| \frac{d\,ln(n_e^2)}{dt} \right|. \tag{17}$$

The assumption in Eq. (16) requires that the electron-ion recombination coefficient, α, change much less rapidly than the effect caused by the delayed ionization rates. The change in α due to the electron temperature and three-body effects has been shown to be inadequate for interpreting the

experimental results for the change in α_{eff}. The decayed ionization mechanism provides a good interpretation. This means that the change of α in time ($d\alpha/dt$) due to any reason other than the mechanism of delayed ionization is much smaller than $d\alpha_{eff}/dt$ due to the mechanism of delayed ionization, or Eq. (16).

Equation (17) can be verified by substituting the relevant parameters, which are all measured in the experiment except the α value. To prove the validity of Eq. (17), α is estimated by the effective α_{eff} measured in this work. The effective α_{eff} is a combination of electron-ion recombination (α value) and delayed ionization contributions. Since $|\ d\alpha/dt\ | \ll |\ d\alpha_{eff}/dt\ |$, with the delayed ionization time scale increasing, its contribution to the α value is decreased in time. Thus we conclude that the α value should be larger than α_{eff}, and they become closer for later times when the delayed ionization processes is less important. Based on this conclusion, we can estimate α from the effective α_{eff} that have measured.

For the 16 mTorr TMAE case, α_{eff} increases from 2.1 $\times 10^{-6}$ cm^3/s at t= 1250 ns to 2.8 $\times 10^{-6}$ cm^3/s at t =1750 ns. Since α_{eff} increases with time, $\alpha_{eff} > 3 \times 10^{-6}$ cm^3/s is predicted for later times. Thus, $\alpha > \alpha_{eff} > 3 \times 10^{-6}$ cm^3/s is predicted, based on the conclusion that α value is close to but larger than α_{eff} for later times. The analysis here does not imply that the α value is around 3×10^{-6} cm^3/s, but the α value could be larger, such as 4×10^{-6} cm^3/s or more. A more accurate α value is difficult to predict from this work, but this estimate of a lower bound for the α value is sufficient to verify the assumption in Eq. (17).

The $\dfrac{d\alpha_{eff}/dt}{(\alpha - \alpha_{eff})}$ values can be calculated under the assumption $\alpha = 3 \times 10^{-6}$ cm^3/s or $\alpha = 4 \times 10^{-6}$ cm^3/s. Those results compared with the $d\ln(n_e^2)/dt$ values are shown in Fig. 12, which verifies that Eq. (17) is well satisfied for most cases, especially for higher α values, or at earlier times. The physical meaning for the condition implied by Eq. (17) is that $\alpha - \alpha_{eff}$ varies more slowly in time when compared to the rapidly decaying electron density.

Under the conditions of Eq. (17), the relaxation times τ of the delayed ionization can be calculated from Eq. (14), and the results are shown in Fig. 13. The points on the solid lines are under the condition that $\dfrac{d\alpha_{eff}/dt}{(\alpha - \alpha_{eff})}$ is less than 30% of the $d\ln(n_e^2)/dt$ values when $\alpha = 3 \times 10^{-6}$ cm^3/s (the lower bound) is assumed. The points on the dashed lines do not satisfy this condition, but Eq. (17) could still hold if the α value is larger than 3×10^{-6} cm^3/s, which is quite possible.

Two conclusions can be drawn from the relaxation time results from Fig. 13: (1) the relaxation time of the delayed ionization increases with time; (2) the relaxation time of the delayed ionization decreases with increasing TMAE pressure.

The relaxation time of the delayed ionization, τ, is quite comparable to the lifetime of the TMAE** state, because TMAE** is the source of the delayed ionization. The lifetime of TMAE** can be influenced by the TMAE pressure and electron density due to collisions. Thus, the relaxation time τ is related to TMAE pressures and electron densities.

As the electron density decreases with time, the rate of electron quenching of TMAE** decreases, so that the lifetime of TMAE** and the relaxation time of the delayed ionization increase with time.

As TMAE pressure increases, the rate of TMAE molecular quenching of TMAE** increases, so that the relaxation time decreases.

In sum, with the assumption that electron density change is primarily due to electron-ion recombination and delayed ionization processes, a model is developed to calculate the relaxation time of the delayed ionization, which are longer under lower TMAE pressures and lower electron densities.
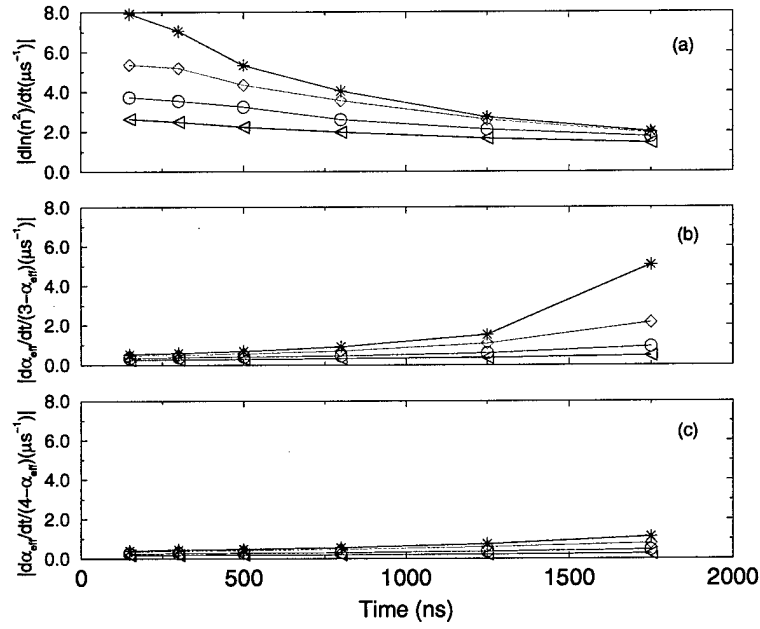
17

Figure 12: (a) $\mid d\,ln(n_e^2)/dt \mid$ versus time; (b) $\mid \frac{d\alpha_{eff}/dt}{(k-\alpha_{eff})} \mid$ versus time with the assumption of $k = 3 \times 10^{-6}$ cm^3/s; (c) $\mid \frac{d\alpha_{eff}/dt}{(k-\alpha_{eff})} \mid$ versus time with the assumption of $k = 4 \times 10^{-6}$ cm^3/s. The data are under conditions of 4 mJ/cm^2 laser fluence with TMAE pressures of ($\star$) 16 mTorr, ($\diamond$) 8 mTorr, (o) 4 mTorr, and ($\triangleleft$) 2 mTorr.
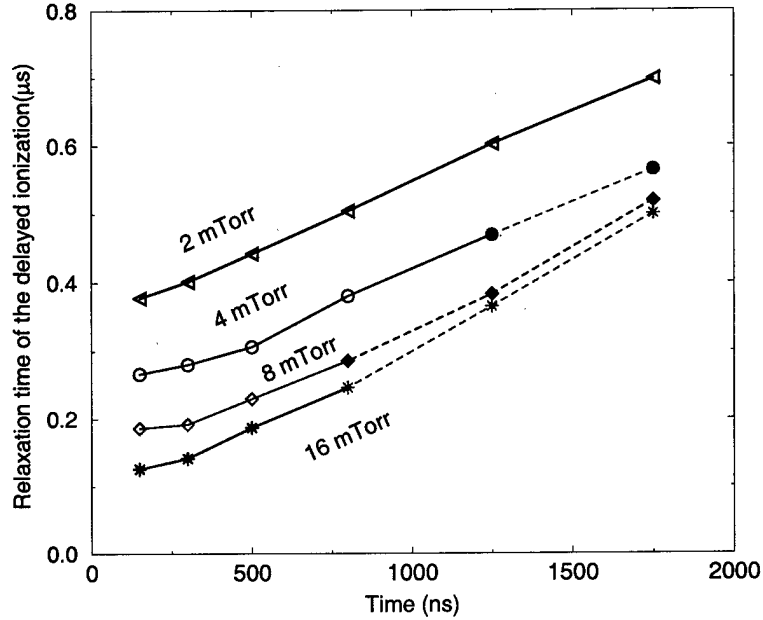
Figure 13: The relaxation times of the delayed ionization calculated from for Eq. (14). The data are under conditions of 4 mJ/cm^2 laser fluence with TMAE pressures of ($\star$) 16 mTorr, ($\diamond$) 8 mTorr, (o) 4 mTorr, and ($\triangleleft$) 2 mTorr.

2.6 Summary

A fast Langmuir probe technique is developed to diagnose the decay process of a laser-produced TMAE plasma, which has a large volume (hundreds of cm^3), high density (10^{13}/cm^3 - 10^{12}/cm^3) and low electron temperature ($\sim$ 0.1 eV). and TMAE pressure. The plasma density decay more rapidly for higher TMAE pressure and electron densities.

In this experiment, the apparent electron-ion recombination coefficient is found to increase with time, and the higher TMAE pressure, the faster the increase. But the change of the recombination coefficient is only weakly dependent on electron temperature. The optical experiments show that nitrogen can enhance the delayed emission from a TMAE Rydberg state in TMAE plasma. The analysis compared with the experiments indicates that a delayed ionization after the laser excitation is important in the TMAE plasma decay.

With the assumption that electron density change is primarily due to electron-ion recombination and the delayed ionization processes, a model is developed to calculate the relaxation time of the delayed ionization, which is longer under the lower TMAE pressure and lower electron density.

3 RF plasma sustainment

The introduction of an easily ionized gas to enhance electrical conductivity and help maintain plasma density is common practice. A requirement of the seed gas is that it should be easily ionized, with an ionization energy lower than dissociation energy. Another requirement is that the material should vaporize easily and have a relatively high vapor pressure.

The introduction of TMAE as a seed gas is reasonable in light of the ease of ionization by VUV

radiation. In fact, because TMAE is so easy to ionize, it has long been used as a photocathode [49, 50]. In addition to the presence of compounds which interfere with the seeded plasma, there is an issue of photon absorption cross-sections being decreased with an increase in oxygen concentrations. There appears to be somewhat less VUV absorption in $TMAE/O_2$ than in pure TMAE at a wavelength of 193 nm [51]. The result of this effect is that we might expect somewhat lower initial electron densities in a TMAE-air mixture.

We have experimented with various neutral pressures of TMAE and found that we can produce a high-density plasma with about 60 mTorr of TMAE. The plasma density in this experiment was $4 \times 10^{13}/cm^3$ and was verified by measuring the X-band microwave reflectivity of the plasma, as well as by Langmuir probe measurements. We also found that the high-density plasma could be formed with 60 mTorr of TMAE and 760 Torr of total pressure when the remainder of the filling gas was helium. This suggested that it may be possible to create and maintain this high-pressure plasma in atmospheric air.

Code simulations using ANTENA2 and MAXEB suggest that with a smaller diameter chamber and a Nagoya-III antenna, a significant radiation resistance could result, and efficient power coupling to the plasma could be achieved. An experiment was done to see what pressure of atmospheric air could be used, and still maintain a discharge. It was found that a plasma with a density of $10^{11}/cm^3$ and length of 30 cm could be maintained at pressures of up to 20 Torr. At pressures above 20 Torr, we found that the antenna could not initiate the discharge.

At this point we turned to the addition of TMAE to the chamber. The first test was to see if we could initiate the radiofrequency discharge above 20 Torr with a small amount of TMAE present. It seemed plausible considering the ionization energy of TMAE is significantly lower than that of nitrogen and oxygen. What we found, however, was that the discharge could not be initiated at a pressure above 4-6 Torr. It seems that the complexity of collisions associated with TMAE reduced the efficiency of power coupling to the discharge.

The second test, however, showed great promise. We hypothesized that if we could initiate the discharge with the 193 nanometer laser, we could couple RF power to the plasma through our antenna and maintain a higher density. This method has proved effective at pressures of at least 100 Torr.

Figures 14 and 15 show the experimental setup. The laser enters the chamber through a VUV window, and ionizes a fraction of available TMAE molecules. The RF antenna in the photo is a twisted double helix. ANTENA codes showed this regime to be the best at coupling RF power in the mid to high pressure ranges (1-1000 Torr). In designing the antenna, it is important to keep in mind that the inductance of the antenna is proportional to it's length. In order to maintain a high Q value for this antenna, the inductance was kept to a minimum. Meanwhile, the losses in the antenna arise primarily from connection points and solder points. So total antenna length is less important when considering surface losses and continuous copper pieces were utilized whenever possible.

The millimeter wave interferometer shown in the experiment is a 104 GHz Gunn oscillator. The system is tuned such that a sensitivity for density measurements is of the order $10^{12}/cm^3$. Measurements of the plasma density using both Langmuir probes and the interferometer show that densities of the order $10^{13}/cm^3$ are achieved in 1-20 Torr of argon and neon. An increase in density is noted when there is a steady state flow through the chamber of the working gas. At higher pressures, the probe interpretation is used only as a qualitative measure to confirm that there is still plasma present, but collisions in the sheath and the finite probe size complicate the interpretation of the signal. For this reason, only the interferometer measurements are used at pressures above 20 Torr, and even in this case, only an approximation to plasma densities can be
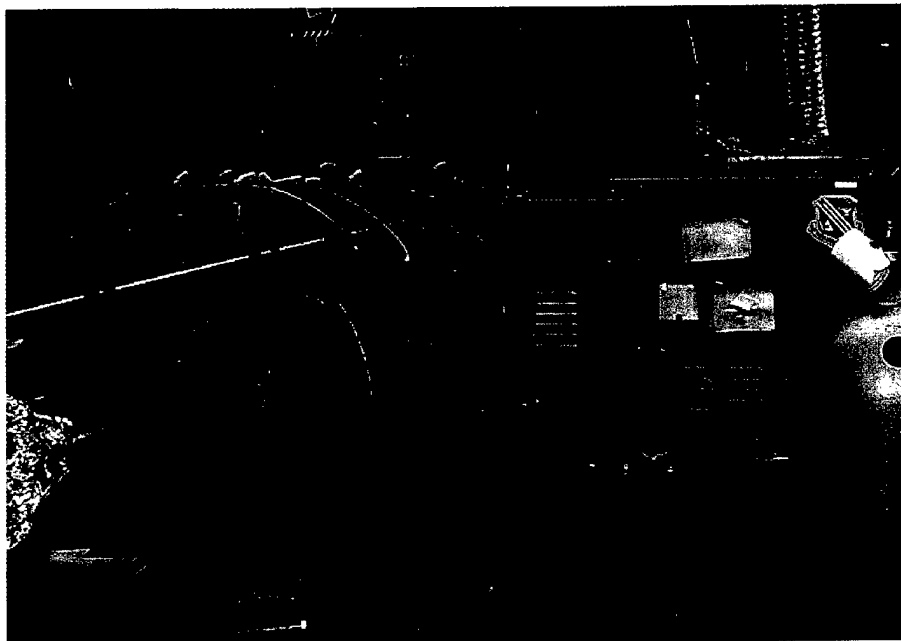
20

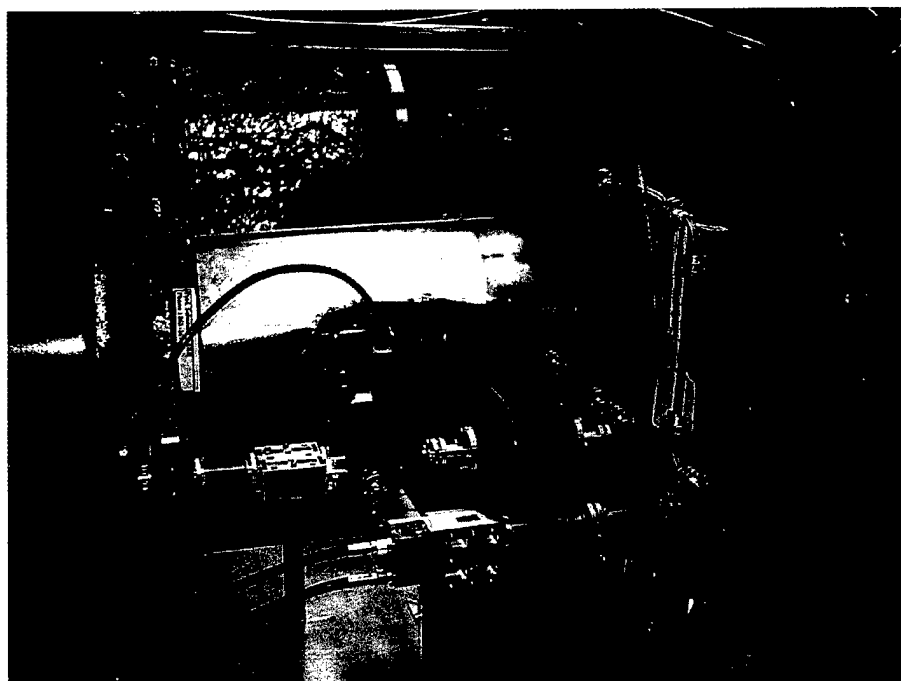Figure 14: Laser and RF plasma apparatus

Figure 15: Millimeter wave interferometer for measuring RF plasma

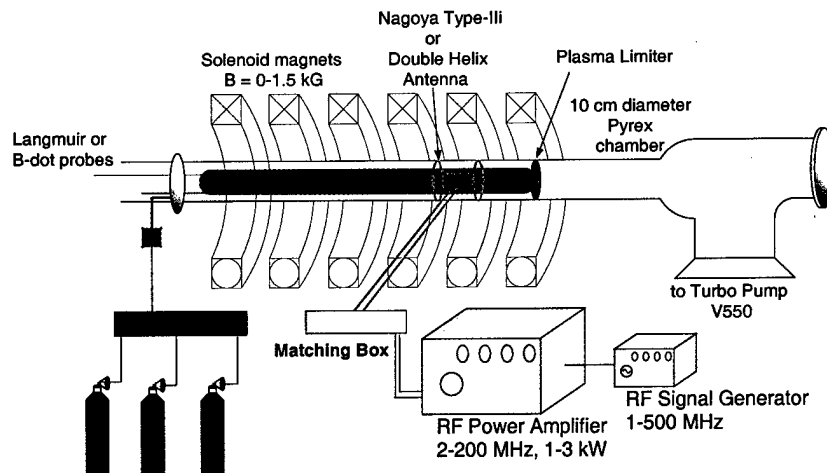Figure 16: Experimental setup for rf production of plasma.

determined due to the complexity of collisions. Plasma densities of the order $10^{12}/cm^3$ have been measured with this interferometer in 760 Torr of argon, and significant density has been confirmed using a Langmuir probe in both 400 Torr of air, and a mixture of TMAE and air. The coupled rf absorbed power density to sustain these plasmas is $P_{abs} = 0.3$ W/cm^3.

In addition, magnetic field effects were measured for this regime. Although the magnetic field did enhance mid and low pressure plasma discharges, the effects diminished as the pressure increased until there was no measurable effect in the high pressure range (above 100 Torr). Several magnetic field configurations were used in the experiment including a sharp gradient field produced by reversing one of the coils, and near uniform field by placing the coils close together with the polarity checked in both directions. In some low pressure cases, the sharp density gradient made the discharge easier to initiate, and the radiation resistance was effected, but as the pressure range increased, these effects diminished.

# 4 Radiofrequency Plasma Source

We have constructed a radio frequency helicon plasma source facility which is schematically shown in Fig. 16. The plasma chamber is a 10 cm (diameter) × 120 cm (length) cylindrical pyrex pipe and is pumped to a base pressure of 3 × 10^{-7} Torr by a 550 l/s turbo molecular pump. A DC magnetic field up to 2 kG is provided by a set of five solenoid coils. We have examined two types of axial magnetic field configurations, i.e. uniform magnetic field and magnetic field with a strong gradient at one end of the coupling antenna. The strong gradient case assists wave absorption and ionization.

Argon, nitrogen, and oxygen gases are fed into the chamber via flow controllers and a mixer through a radial port. A 2-200 MHz 1 kW rf power amplifier is connected to a Nagoya Type III or a half-turn double helix antenna (15 cm long) through a matching network to couple RF power to the plasma. The Nagoya Type III and half-turn double helix antennas are shown in Fig. 17.

Langmuir probe, B-dot magnetic wave field probe and diamagnetic loop diagnostics have been used in the past to study axial and radial plasma density profiles, axial electron temperature profile, wave propagation, and transverse plasma temperature characteristics. The recent addition of an Ocean Optics ST2000 fiber optic spectrometer allows us to examine the spectral emissions of our
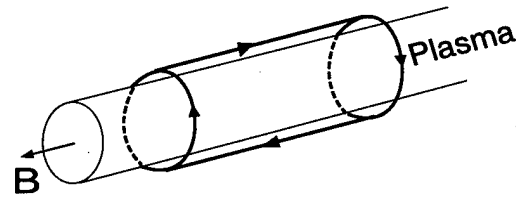
Nagoya Type-III
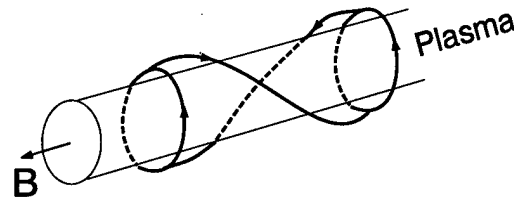
Half-Turn Double Helix

Figure 17: Diagram of antenna types used in the rf experiments. Each antenna has a length of 15 cm.

plasmas over the 200-800 nm frequency range.

We have carried out experiments in nitrogen/argon gas mixtures at 1 Torr with a half-turn double helix antenna and uniform magnetic field (B_0 = 1400 G), obtaining plasmas with cylindrical volumes of 7000 cm^3. We examined different nitrogen/argon gas concentration at 1 Torr, scanning seed gas constituents from 35% Ar with 65% N_2 up to 75% Ar with 25% N_2. For reference, the spectral emissions of a pure Nitrogen plasma at 1 Torr and a pure Argon plasma at 1 Torr are shown in Figures 18 and 19, respectively. We find that if we have more than 50% nitrogen in our concentration, the N_2 dominates, giving us a weak pinkish color plasma, that is strongest under the antenna, and extends (< 20 cm) away from the antenna.

The spectral emission of this Nitrogen dominated plasma is shown in Fig. 20, which clearly shows N_2 lines similar to those of the pure N_2 case. Similarly, if we have more than 70% argon, the Ar dominates, giving us a purple color plasma that is strongest under the antenna, extends (< 20 cm) in one direction, and extends 30 cm in the other direction. However, in the range of 50%/50% to 40%/60% of N_2/Ar, we see a stronger orange/yellow color plasma, that is very intense under the antenna, and extends axially for 0.75 m. The spectral emission of a plasma in this regime is shown in Fig. 21, and it can be seen that both Argon and Nitrogen lines are prominent. There is a distinct improvement in plasma size and plasma resistive loading for this N_2/Ar mix in comparison with either the pure Ar or pure N_2 cases. The combination of both nitrogen and argon spectral emission lines along with the improved plasma characteristics implies that a positive seed gas effect occurs in this N_2/Ar concentration range. Figure 22 shows the plasma created for the 35% N_2/65% Ar 1 Torr case.

Figure 23 illustrates the optimum case of power reflection from the half-turn double helix antenna with a capacitive matching system driven at 9.26 MHz. The forward and reflected power is measured using a calibrated Bird meter. In this case, the gas mixture is 35% nitrogen and 65% argon at 1 Torr in a static magnetic field of 1.4 kG. Reflected power is 17%, indicating efficient power coupling for this type of antenna at pressures of 1 Torr. After taking into account the
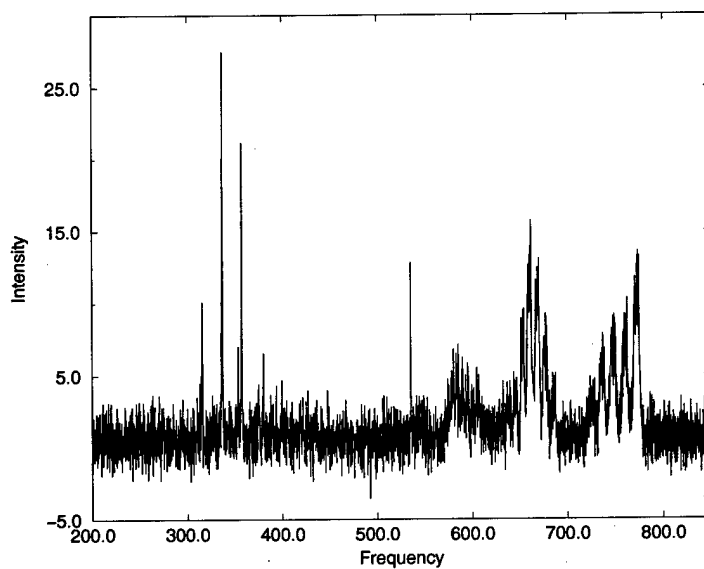
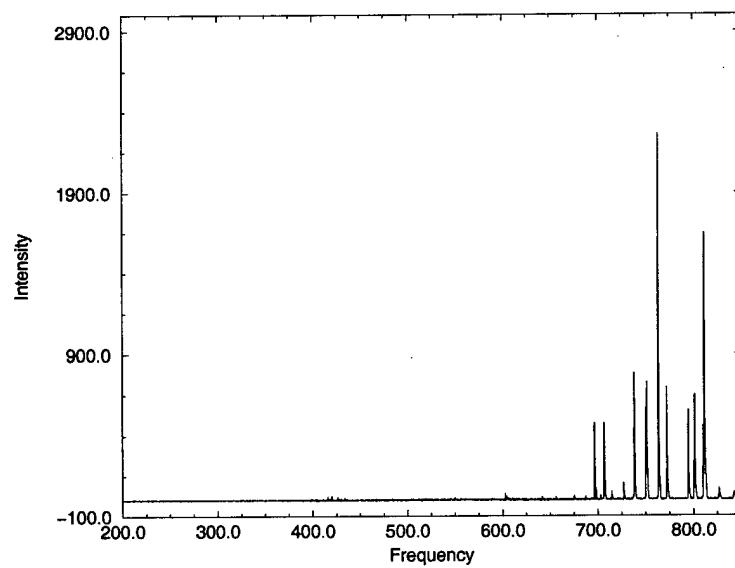Figure 18: Spectral emission lines for a pure Nitrogen plasma at 1 Torr.

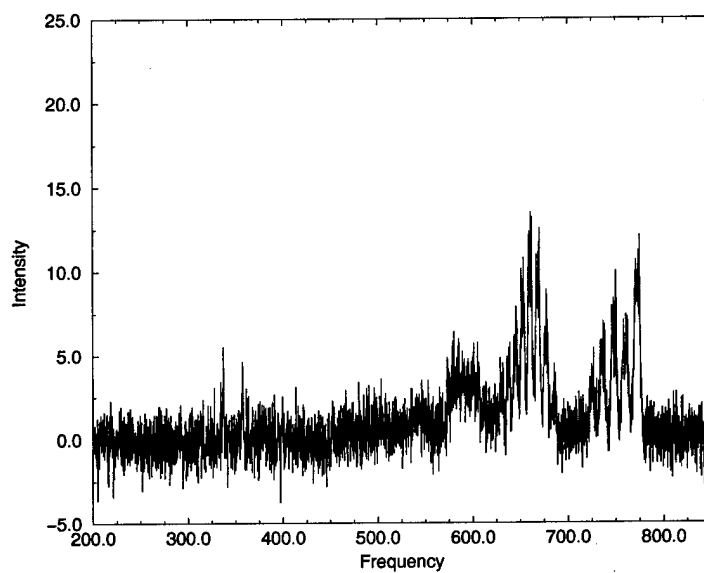Figure 19: Spectral emission lines for a pure Argon plasma at 1 Torr

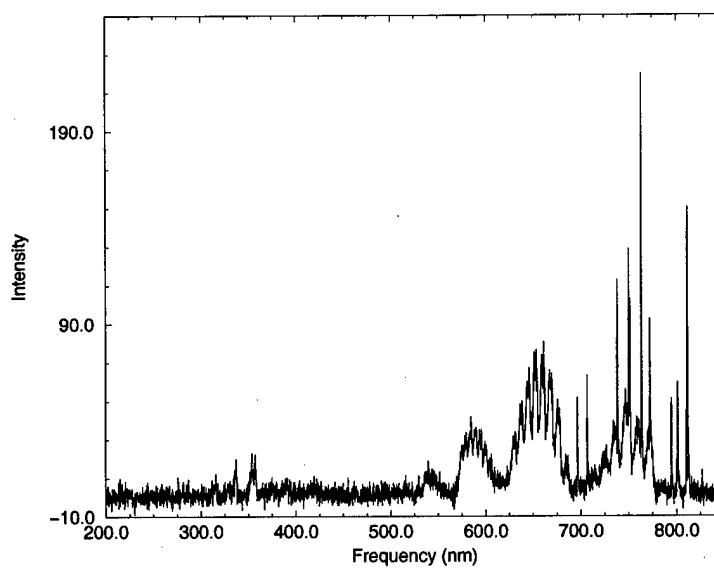Figure 20: Spectral emission lines of Nitrogen dominated ($N_z > 50\%$ plasma at 1 Torr.

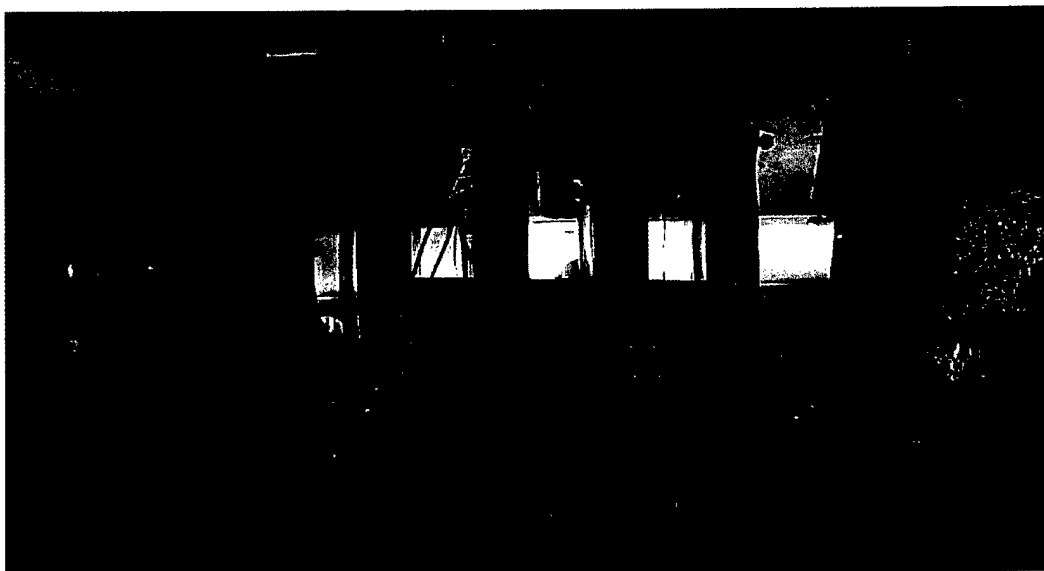Figure 21: Spectral emission lines of 65% AR/35% N_2 plasma at 1 Torr.

Figure 22: Mix plasma at 1 Torr.

antenna and plasma losses, we calculate a net power coupled to the plasma of 250 W. This implies that the power density needed to sustain the plasma at optimum mix of 40% nitrogen with 60% argon at 1 Torr is 0.04 W/cm^3.

The impedance of the half-turn double helix antenna is measured using a network analyzer, and the conjugate match principle is utilized. For the optimum match 1 Torr case, the antenna plasma impedance is measured to be $Z_{antenna} = 0.3 + j4$ Ω. Note that this compares very closely to the ANTENA-II code simulation values of $Z_{antenna} = 0.28 + j1.6$ Ω for a $5X10^{12}$ /cm^3 density plasma at 1.4 kG and 1 eV temperature. This code has been used with success in earlier experimental comparisons and we will use it to scale to higher pressure cases.

5   Simulation of High Pressure Air Plasmas by Inductive Codes

The effects of the DC magnetic field , rf frequency, electron density, collision rates and antenna configuration on power coupling in high pressure plasmas have been studied by using the ANTENA-II and MAXEB codes developed by our group [6, 3, 4]. The inductive coupling problem for different types of antenna coils is solved numerically in these codes. Plasma density and temperature radial profiles are included in the 1-D ANTENA-II code, while nonuniformity of plasma density, temperature and DC magnetic field in both r and z directions can be treated in the 2-D MAXEB code. We have previously examined lower pressure (1-10 mTorr) rf helicon wave coupling and collisional and collisionless wave absorption using the ANTENA-II and MAXEB codes. The comparison between simulation and experiment results for Argon plasma at 1 mTorr with uniform and nonuniform DC magnetic field has been carried out with good agreement for both field solutions and antenna-plasma impedance [4].

The effect of DC magnetic fields on the power absorption profile for a Nagoya-III type antenna at a collision rate of $\nu = 10^9$ 1/s is shown in Fig. 24. The collision rate is indicative of high neutral gas pressure and is taken to be $\nu = 3 \times 10^9 \times P$ (Torr). Note that actual collision rates in air mixtures can vary by factors of order five times lower than this due to the detailed nature of the electron distribution function. The figure shows that the radial wave penetration into the plasma is
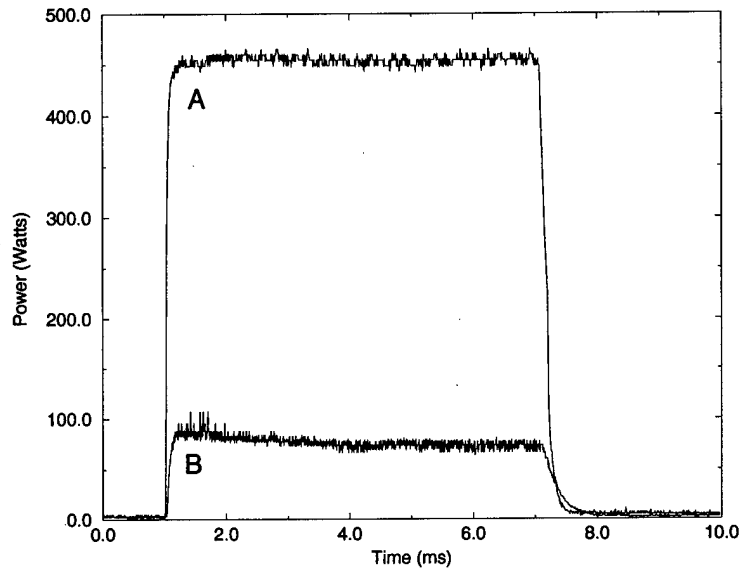
Figure 23: Forward (A) and reflected (B) power for the half-turn double helix antenna coupling rf power to the Ar/N mix plasma at 1 Torr. Reflected power = 17%.

enhanced for the same density and collision rates as the magnetic field is increased. The radiation resistance versus the DC magnetic field for the same collision rate is shown in Fig. 25. It's noted that the radiation resistance is also increased with increasing magnetic field, which is helpful in the matching the antenna to the RF generator and overcoming skin effect losses in matching and coupling circuit.

The effect of varying the rf frequency on the radiation resistance is shown in Fig. 26. We found that an increase in the frequency helps to increase the radiation resistance substantially. A roughly linear dependence of R_r on frequency can be observed from the diagram. We believe that the frequency increase causes a significant increase in the field magnitude at the edge of the plasma for the same power input, therefore it increases the power coupling efficiency. Although substantial radiation resistances can be achieved in the code simulation, matching at these high frequencies is experimentally challenging. Air core or ferrite transformers which insure a balanced rf current drive on the antenna are required. So in practice, it is desirable to find an optimum frequency at which both a substantial radiation resistance and good matching techniques can be obtained.

The effect of the plasma peak density variation on the antenna radiation resistance is illustrated in Fig. 27 for an antenna driven at 13.56 MHz and a magnetic field of 1 kG for high pressure ranges corresponding to 100-1000 Torr. The radiation resistance varies from 0.0038 Ohms at $10^{12}/cm^3$ density to 0.44 Ohms at $10^{15}/cm^3$ density with the neutral pressure in the 100 Torr range. The radiation resistance increases substantially with density and is reduced as the collisionality is increased. We found that high electron density plays an important role in getting efficient power coupling at high pressures. This notion will help us build a new experimental device with both laser initiation and rf sustainment heating to create a steady state plasma with densities of $10^{13}/cm^3$ at atmosphere air pressures. The use of Argon and organic seed gases and laser preionization will greatly assist this experiment.
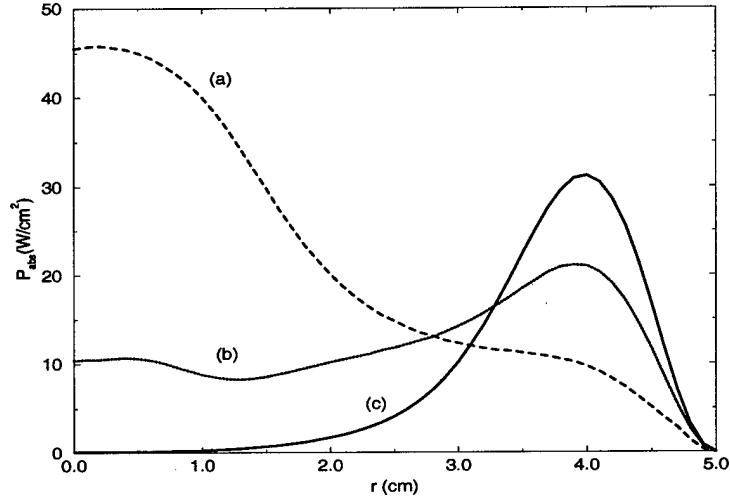
Figure 24: The effect of the magnetic field on the radial power absorption profile. (a) B=10,000 G, (b) B=2000 G, (c) B=500 G with $n_0 = 10^{14}/cm^3$, f=13.56 MHz and $\nu = 10^9$ 1/s.

Figure 25: The effect of magnetic field on the antenna radiation resistance. $n_0 = 10^{14}/cm^3$, f=13.56 MHz and $\nu = 10^9$ 1/s.

Figure 26: The effect of frequency on the antenna radiation resistance. $n_0 = 10^{14}/\text{cm}^3$, B=1000 G and $\nu = 10^{11}$ 1/s.

Figure 27: The effect of plasma peak density on the antenna radiation resistance. (a) $\nu = 10^{11}$ 1/s, (b) $\nu = 10^{12}$ 1/s with B=1000 G and f = 13.56 MHz.

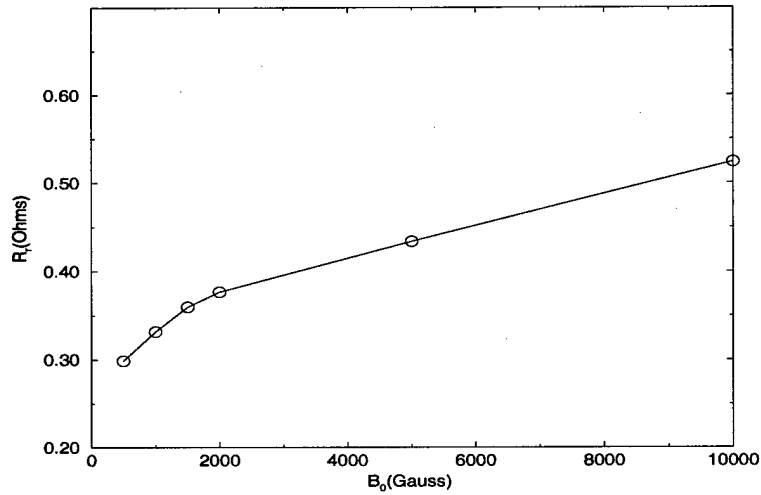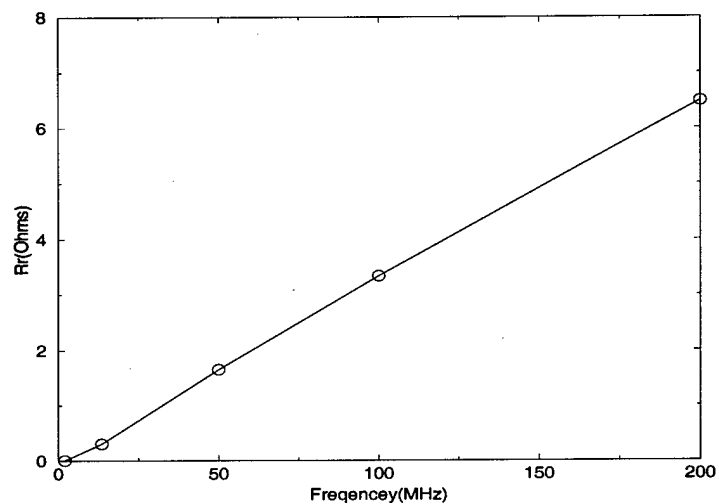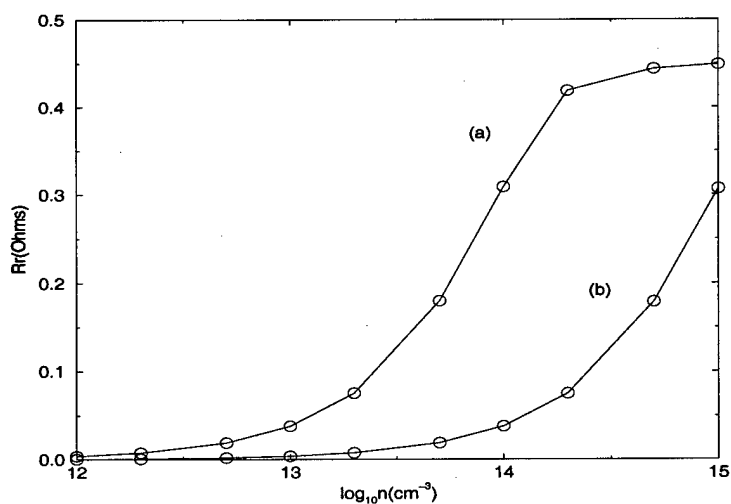Experimentally, we have produced a mixed Nitrogen-Argon plasma at 2 Torr. The measured antenna radiation resistance is 0.3 Ohms. The reactance measured at the feed points is 4.3 Ohms. The plasma reactance is determined to be 2.6 Ohms after making correction for the feeds and vacuum antenna reactance. The electron-Argon neutral collision rate and electron-Nitrogen neutral collision rate at 2 Torr are $\nu_{e-Ar} = 1.6 \times 10^8$ 1/s and $\nu_{e-N2} = 3.0 \times 10^9$ 1/s, respectively [52]. We ran ANTENA-II and obtained R_r=0.25 Ohms, X_r=4.5 Ohms at $n_e = 3.0 \times 10^{12}$/cm^3 for Ar, and R_r=0.32 Ohms, X_r=4.4 Ohms at $n_e = 1.0 \times 10^{13}$/cm^3 for N_2. By using the code to pinpoint both the antenna resistance and reactance values, we determined the density range for our 2 Torr $N_2 - Ar$ plasma to be $3 \times 10^{12} - 10^{13}$/cm^3 at 1 eV.

We have also made a comparison between the atmosphere air pressure plasma experiment by Eckert et al. [53] and the Thomson model [54, 55]. Plasma flames in air with an average $n_e = 5 \times 10^{14}$/cm^3 were produced at the atmosphere pressure by rf induction. The power dissipated is P_{rf}=18 kW, the rms values of coil current and voltage are 40 A and 3.5 kV at a rf frequency of 4 MHz. The plasma radiation resistance is determined to be 11.3 Ohms based on the reported experimental data. The power absorbed by the plasma in Thomson model is calculated as

$$P_{abs} = 2\pi R l S_{abs},$$

where R and l are the radius and length of the plasma, respectively, and S_{abs} is the magnitude of the Poynting vector at the boundary and

$$S_{abs} = H_{z0}^2 \frac{\pi \omega \mu_0 R}{\beta R} Re[\frac{j^{1/2} J_1(-j^{1/2}\beta R)}{J_0(-j^{1/2}\beta R)}],$$

where β is the radial wave number in the plasma.

We utilized this model to calculate the power absorbed by the plasma and then obtained the resistance value to be 11.28 Ohms at $\nu = 2.3 \times 10^{12}$, which is indicative of the atmosphere pressure. This good agreement indicates that Thomson model can describe the high pressure plasma power coupling with large skin depths very well and is used to interpret our high air pressure rf plasma sustainment.

References

[1] G. Ding, J. E. Scharer, and K. Kelly. Effects of rapidly decaying plasma on Langmuir probe measurements. *J. Appl. Phys.*, 84(3):1236, 1998.

[2] K. Kelly, J. E. Scharer, and G. Ding. Microwave reflections from a vacuum ultraviolet laser produced plasma sheet. *J. Appl. Phys.*, 85(1):63, 1999.

[3] Y. Mouzouris and J. E. Scharer. Wave propagation and absorption simulations for helicon sources. *Phys. Plasmas*, 5(12):4253–4261, Dec 1998.

[4] X. Guo, J. E. Scharer, Y. Mouzouris, and L. Louis. Helicon experiments and simulations in nonuniform magnetic field configurations. *Phys. Plasmas*, 6(8):3400–3407, 1999.

[5] Guowen Ding, John E. Scharer, and Kurt L. Kelly. Diagnostics and analyses of decay processes in laser produced tmae plasmas. *Accepted for publication in the Physics of Plasmas*, page 39, April 2000.

[6] Y. Mouzouris and J. E. Scharer. Modelling of profile effects for inductive helicon plasma sources. *IEEE Trans. on Plasma Sci.*, 24(1):152–160, 1996.

[7] S. P. Bozeman and W. M. Hooke. Magnetically enhanced electromagnetic wave penetration in weakly ionized plasmas. *Plasma Sources Sci. Technol.*, 3:99–107, 1994.

[8] Y. S. Zhang and J. E. Scharer. Plasma generation in an organic molecular gas by an ultraviolet laser pulse. *J. Appl. Phys.*, 73(10):4779, 1993.

[9] G. Ding, J. E. Scharer, and K. L. Kelly. Nitrogen influences on a laser produced tmae plasma. *Proceedings of IEEE Plasma Science Conference*, page 199, 1999.

[10] J. E. Scharer, G. Ding, H. Gui, X. Guo, K. Kelly, and E. Paller. Laser and radiofrequency production of seeded air plasmas. *AIAA Plasmadynamics and Lasers Conference*, 1999.

[11] A. Remacle and R. D. Levine. Prompt and delayed ionization on large moledules. *Phys. Lett. A*, 173:284, 1993.

[12] G. Y. Marr. *Photoionization processes in gases*. Academic Press Inc., London, 1967.

[13] G. Ding and J. E. Scharer. Decay process in laser produced TMAE plasma. *manuscript in progress*, 1999.

[14] R. A. Holroyd, S. Dhrnso, and J. M. Preses. *J. Phys. Chem*, 89:4144, 1985.

[15] A. J. T. Holmes, L. M. Lea, A. F. Newman, and M. P. S. Nightingale. *Rev. Sci. Instrum.*, 58(2):223, 1987.

[16] M.A. Biondi. Recombination, page 127—146. In G. Bekefi, editor, *Principles of Laser Plasmas*, chapter 4. John Wiley & Sons, New York, 1976.

[17] M. T. Leu, M. A. Biondi, and R. Johnsen. *Phys. Rev. A*, 7(1):292, 1972.

[18] C. Huang, M. Whitaker, M. A. Biondi, and R. Johnsen. *Phys. Rev.*, A18(1):64, 1978.

[19] G. Y. Marr. *Photoionization processes in gases*. Academic Press Inc., London, 1967.

[20] Y. Nakato, M. Ozaki, and H. Tsubomura. *Bulletin of the chemical society of Japan*, 45:1299, 1972.

[21] A. C. Jones, M. J. Dale, M. R. Banks, I. Gosney, and P. R. Langridge-Smith. *Mol. Phys.*, 80(3):583, 1993.

[22] E. B. Gallogly, Y. Bao, K. Han, H. Lin, and W. M. Jackson. *J. Phys. Chem.*, 98:3121, 1994.

[23] W. G. Scherzer, H. L. Selzle, E. W. Schlag, and R. D. Levine. *Phys. Rev. Lett.*, 72(10):1435, 1994.

[24] R. G. Neuhauser, K. Siglow, and H. J. Neusser. *J. Chem. Phys.*, 106(3):896, 1997.

[25] A. Held, L. Y. Baranov, H. L. Selzel, and E. W. Schlag. *J. Chem. Phys.*, 106(17):6848, 1997.

[26] W. G. Scherzer, H. L. Selzle, and E. W. Schlag. *Z. Fur Naturf. A.*, 48(12):1256, 1993.

[27] C. E. Alt, W. G. Sherzer, H. L. Selzle, and E. W. Schlag. *Ber. Bunsenges. Phys. Chem.*, 99(3):332, 1995.

[28] W. G. Sherzer, H. L. Selzle, E. W. Schlag, and R. D. Levine. *Phys. Rev. Lett.*, 72(10):1435, 1994.

[29] H. Krause and H. J. Neusser. *J. Chem. Phys.*, 99(9):6278, 1993.

[30] M. C. Cockett, H. Ozeki, K. Okuyama, and K. Kimura. *J. Chem. Phys.*, 98:7763, 1993.

[31] D. Tanaka, S. Sato, and K. Kimura. *Chem. Phys.*, 239:437, 1998.

[32] L. A. Pinnaduwage and Y. Zhu. *Chem. Phys. Lett.*, 277:147, 1997.

[33] C. C. Pan, C.C. Chou, C. H. Lu, Y. Tai, and K. C. Lin. *J. Chem. Phys.*, 107(10):3797, 1997.

[34] A. Amrein, R. Simpson, and P. Hackett. *J. Chem. Phys.*, 95(3):1781, 1991.

[35] A. Amrein, R. Simpson, and P. Hackett. *J. Chem. Phys.*, 94(6):4663, 1991.

[36] H. Lin, K.L. Han, Y. H. Ban, E.B. Gallogly, and W. M. Jackson. *J. Phys. Chem*, 98(48):12495, 1994.

[37] K. W. Kennedy and O. Echt. *J. Phys. Chem*, 97:7088, 1993.

[38] F. Negri and M. Z. Zgierski. *J. Chem. Phys.*, 107(13):4827, 1997.

[39] F. Merkt and R. N. Zare. *J. Chem. Phys*, 101(5):3495, 1994.

[40] E. W. Schlag and R. D. Levine. *J. Phys. Chem.*, 96:10608, 1992.

[41] R. D. Levine. *Adv. Chem. Phys.*, 101:625, 1997.

[42] Hiroki Nakamura. *Int. Rev. Phys. Chem.*, 10(2):123, 1991.

[43] E. W. Schlag. *ZEKE Spectroscopy.* Cambridge University Press, Cambridge, 1998.

[44] A. Remacle and R. D. Levine. *Phys. Lett. A.*, 173:283, 1993.

[45] Hitoshi Koizumi. *J. Chem. Phys.*, 95(8):5846, 1991.

[46] M. Hori, K. Kimura, and H. Tsubomura. *Spectrochim. Acta*, A 24:1397, 1967.

[47] Y. Nakato and H. Tsubomura. *J. Luminescence*, 76(15):2105, 1976.

[48] H. Weingarten and W. A. White. *J. Org. Chem.*, 31:3427, 1966.

[49] T. M. Freeman and W. R. Seitz. Oxygen probe based on tetrakis(alkylamino)ethylene chemiluminescence. *Anal. Chem.*, 53:98–102, 1981.

[50] K. Kuwata and D. H. Geske. The cation radical of tetrakis(dimethylamino)ethylene. *Journal of the American Chemical Society*, 86(11):2101, 1964.

[51] S. Toby, P. A. Astheimer, and F. S. Toby. Chemiluminescence in the gas phase reaction between tetrakis(dimethylamino)ethylene and oxygen. *Journal of Photochemistry and Photobiology A-Chemistry*, 67(1):1–12, 1992.

[52] D.Ẽ. Golden. Low-energy resonances in $e^- - n_2$ total scattering cross sections: The temporary formation of n_2^-. *Phys. Rev. Lett.*, 17(16):847–848, 1966.

[53] H. V. Eckert, F. L. Kelly, and H. N. Olsen. Spectroscopic observations on induction - coupled plasma flames in argon and air. *Journal of Applied Physics*, 39:1846–1852, 1968.

[54] J. J. Thomson. *Phil. Mag.*, 32:321–445, 1891.

[55] M. A. Lieberman and A. J. Lichtenberg. *Principles of Plasma Discharges And Materials Processing.* John Wiley and Sons, Inc., New York, 1994).

6 Journal Publications (1998–2000)

1. G. Ding, J. Scharer, K. Kelly, "Decay Process in Laser Produced TMAE Plasma," accepted for publication in the *Physics of Plasmas*, March 2000.

2. X. Guo, J. E. Scharer, Y. Mouzouris and L. Louis, "Helicon Experiments and Simulations in Nonuniform Magnetic Field," Physics of Plasmas **6** (8), 3400–3407 (1999).

3. Y. Mouzouris and J. E. Scharer, "Two-Dimensional (r,z) Plasma Wave Absorption and Poynting Flux Simulations for Helicon Sources," Special Issue – *Images in Plasma Science, IEEE Trans. of Plasma Science* **27** (1), 66–67 (1999).

4. K. L. Kelly, J. E. Scharer, G. Ding, M. Bettenhausen and S. P. Kuo, "Microwave Reflections from a Vacuum Ultraviolet Laser Produced Plasma Sheet," *Journal of Applied Physics* **85** (1), 63–68 (1999).

5. Y. Mouzouris, and J. E. Scharer, "Wave propagation and Absorption simulations for Helicon sources," *Physics of Plasmas* **5** (12), 4253–4261 (1998).

6. G. Ding, J. E. Scharer, and K. L. Kelly. "Fast Langmuir Probe Measurements in a Laser Produced Plasma," *Journal of Applied Physics* **84** (3), 1236 (1998).

7 Conference Papers (1998–2000)

1. J. Scharer, G. Ding, H. Gui, K. Kelly, E. Paller, "Laser Initiation and Radiofrequency Sustainment of Seeded Air Plasmas," *Bull. Am. Phys. Soc.*, **44**, 67 (1999).

2. K. L. Kelly, J. E. Scharer, G. Ding, H. Gui and E. Paller, "Radio-frequency Sustainment of a Laser-Produced Plasma," IEEE International Conference on Plasma Science, Monterey, June 20-24, Record 99CH36297, 118 (1999).

3. J. Scharer, G. Ding, X. Guo, H. Gui, K. Kelly and E. Paller, "Laser and Radiofrequency Wave Creation of Seeded Air Plasmas," IEEE International Conference on Plasma Science, Monterey, June 20-24, Record 99CH36297, 118 (1999).

4. G. Ding, J. E. Scharer and K. L. Kelly, "Nitrogen Influences On A Laser Produced TMAE Plasma," IEEE International Conference on Plasma Science, Monterey, June 20-24, Record 99CH36297, 199 (1999).

5. J. E. Scharer, X. Guo, L. Louis, Y. Mouzouris and H. Gui, "Broadband Helicon Experiments and 2-D Plasma Profile Simulations," Gaseous Electronics Conference, Maui, Hawaii, Bulletin of the American Physical Society **43**, 1503 (1998).

6. K. L. Kelly, J. E. Scharer and G. Ding, "A Laser-Produced Plasma Sustained by a Radiofrequency Source," IEEE International Conference on Plasma Science, Monterey, June 20-24, Record 99CH36297, 199 (1999).

7. J. E. Scharer, X. M. Guo, K. L. Kelly and H. Gui, "High Pressure N_2, O_2 and Air Mixture Plasmas Produced by a Radiofrequency Helicon Plasma Source," IEEE International Conference on Plasma Science, Monterey, June 20-24, Record 99CH36297, 200 (1999).

8. J. Scharer, G. Ding, H. Gui, X. Guo, K. Kelly, and E. Paller, "Laser and Radiofrequency Production of Seeded Air Plasmas." *AIAA 99–3668*, Norfolk, VA, *30th AIAA Plasmadynamics and Lasers Conference.* June 28–July 1, 1999.

9. J. E. Scharer arranged, organized and was the session chair for two of the three air plasma sessions at the 1998 IEEE-ICOPS, Raleigh, North Carolina, June 1-4, 1998. He also organized and chaired the 1999 session at Monterey, CA.

10. K. L. Kelly, J. E. Scharer, G. Ding, M. H. Bettenhausen. APS-DPP poster presentation. "Microwave Scattering Measurements from a Laser Produced Plasma Sheet." *bMoaP1* Pittsburgh, PA, *APS-DPP conference record* **BAPSDPP97**, 16 (1997).

11. Y. Mouzouris, J. E. Scharer, and M. Bettenhausen, "Two-Dimensional Plasma Wave Field and Absorption Simulations for Helicon Plasma Sources," oral presentation *1A05*, IEEE International Conference on Plasma Science, Raleigh, North Carolina, *IEEE Conference Record* **98CH36221**, 28 (1998).

12. J. E. Scharer, M. Bettenhausen, G. Ding, H. Gui, X. Guo, K. Kelly, and Y. Mouzouris, "Laser and Radiofrequency Tailored Gas Plasma Sources," oral presentation *5C04*, IEEE International Conference on Plasma Science, Raleigh, North Carolina, *IEEE Conference Record* **98CH36221**, 81 (1998).

13. G. Ding, J. E. Scharer, and K. L. Kelly, "Laser Produced TMAE Plasma in Nitrogen, Oxygen, and Air," poster presentation *6P29*, IEEE International Conference on Plasma Science, Raleigh, North Carolina, *IEEE Conference Record* **98CH36221**, 96 (1998).

14. K. L. Kelly, J. E. Scharer, and G. Ding, "Microwave Reflections from a Vacuum Ultraviolet Laser Produced Plasma Sheet," poster presentation *6P30*, IEEE International Conference on Plasma Science, Raleigh, North Carolina, *IEEE Conference Record* **98CH36221**, 96 (1998).

15. X. Guo, J. E. Scharer, H. Gui, and Y. Mouzouris, "Radiofrequency Helicon Plasmas Produced in Air with Concentrations of Nitrogen and Oxygen," poster presentation *6P31*, IEEE International Conference on Plasma Science, Raleigh, North Carolina, *IEEE Conference Record* **98CH36221**, 96 (1998).

16. Y. Mouzouris, J. E. Scharer, and H. Gui, "One and Two Dimensional Plasma Wave Field and Absorption Simulations for Collisional Radiofrequency Air Plasma Sources," poster presentation *6P32*, IEEE International Conference on Plasma Science, Raleigh, North Carolina, *IEEE Conference Record* **98CH36221**, 96 (1998).

17. J. E. Scharer, M. Bettenhausen, G. Ding, H. Gui, X. Guo, K. Kelly, and Y. Mouzouris, "Laser and Radiofrequency Air Plasma Sources," oral presentation *7C05*, IEEE International Conference on Plasma Science, Raleigh, North Carolina, *IEEE Conference Record* **98CH36221**, 105 (1998).

18. K. L. Kelly, J. E. Scharer, G. Ding, M. H. Bettenhausen and N. T. Lam, "Microwave Reflections from a VUV Laser Produced Plasma Sheet," IEEE International Conference on Plasma Science, San Diego, *IEEE Conference Record* **97CH36085**, 134 (1997).

19. G. Ding, J. E. Scharer, K. L. Kelly, M. H. Bettenhausen and N. T. Lam, "Dynamics of a Laser Produced Plasma for Microwave Reflection," IEEE International Conference on Plasma Science, San Diego, *IEEE Conference Record* **97CH36085**, 133 (1997).

20. J. E. Scharer, K. L. Kelly, G. Ding, and M. H. Bettenhausen, "VUV Laser Plasma Formation and Microwave Agile Mirror/Absorber," IEEE International Conference on Plasma Science, San Diego, *IEEE Conference Record* **97CH36085**, 157 (1997).

21. M. H. Bettenhausen, J. E. Scharer, Y. Mouzouris, and K. Kelly "Investigation of RF Effects on Laser Produced Plasmas,," IEEE International Conference on Plasma Science, San Diego, *IEEE Conference Record* **97CH36085**, 202 (1997).

22. Y. Mouzouris, J. E. Scharer, and M. H. Bettenhausen, "Antenna Coupling and Absorption Mechanisms in a Helicon Source Operation," IEEE International Conference on Plasma Science, San Diego, *IEEE Conference Record* **97CH36085**, 202 (1997).

8   Grant Modalities

During the grant period, May, 1997 – April, 2000, the participants carrying out the research were as follows:

- John E. Scharer, Professor

- Dr. M. Bettenhausen, Postdoc (1997)

- Dr. X. Guo, Postdoc (1997-99)

- G. Ding, Graduate Student (Ph.D., graduated 12/99)

- K. Kelly, Graduate Student (Ph.D. program)

- E. Paller, Graduate Student (Ph.D. program)

- Y. Mouzouris (Ph.D., graduated) and H. Gui (Ph.D. program), graduate students who are supported by an NSF grant have also made contributions to this AFOSR research.

- R. Cao, Graduate Student (M.S. Program)

- S. Fusi, Minority Undergraduate Research Student (1997)

- A. Yu, Undergraduate Research Student (1998)

- J. Lauer, Undergrad Research Student (1999-2000)

- We have also collaborated with Prof. S. Kuo (Journal publication) and Dr. C. Laux (Chemical Kinetics code) during this period.

- Professor Scharer has also organized and chaired two air plasma sessions as part of the 1998 and 1999 IEEE International Conference on Plasma Sciences as part of this research.

9 Student Training

During the past three years, May 1, 1997 – April 30, 2000, the participants carrying out the research are as follows:

- John E. Scharer, Professor; Dr. X. Guo, Postdoc
- G. Ding, K. Kelly, and E. Paller, H. Gui, Ph.D. Graduate Students
- R. Cao, M.S. Graduate Student
- Alex Yu, Undergraduate Research Student

The experimental and computational research involves graduate and undergraduate students in the area of laser and radiofrequency formation of air plasmas. It has important potential AFOSR applications such as reduction of radar cross sections, use as a fast (2 ns) shutter for radar turn-off, elimination of biological contaminants and thin film creation in air. The experiments the students participated in include VUV excimer laser formation of a high density organize seed plasma and measurement of the effects of nitrogen, oxygen and other air plasma components on the plasma density and lifetime. They also participated in radiofrequency sustainment and magnetic field effects on the production of collisional air plasmas. The detailed design of radiofrequency coupled diagnostic measurements of plasma properties, measurements of millimeter wave transmission, flash tube plasma production and spectroscopy will be carried out by the students with the Principal Investigator as well as Ph.D. scientists who work on the research. The use of our new turbo molecular higher vacuum system and RGA diagnostics will greatly improve their knowledge of state-of-art vacuum systems and very precise vacuum and gas constituent information can be obtained. Computer simulations of the plasma production by laser and radiofrequency sustainment, the effects of magnetic fields, the diffusion and interaction with microwaves has been developed and an extension of this to analyze data and determine the air and plasma parameters will be extended. Professor Scharer has offered a course, Computational Methods in Electromagnetics, which will be offered again and is of great benefit to the graduate students.

10 Computational Simulations

We are utilizing the extensive computational facilities of the Center for Plasma Theory and Computation (J. Scharer, Co-Director) for simulations of laser and radiofrequency plasma formation, gas constituent ionization, diffusion and recombination as well as the millimeter wave interactions with the medium. The accurate measurement of the gas constituents allows much more accurate models to be developed and used to examine possible improvements in the plasmas created. The computing resources of our Center for Plasma Theory and Computation currently include a Sun Ultra 2 Model 2300 (two 300 MHz CPU's) with 1.28 GB of memory, a Sun Ultra 2 Model 2200 (two 200 MHz CPU's) with 896 MB of memory, a Sun Ultra 2 Model 1170 (two 200 MHz CPU's) with 384 MB of memory, and two Sun SPARCstations 10 (dual 125 MHz hyperSPARC CUP's) with 160 MB of memory. These systems are configured with a combined total of more than 40 GB of hard disk storage. This arrangement facilitates high performance distributed serial and parallel computing. The combined computing power of these seven workstations is more than 25 percent greater than the computing power of a single processor CRAY 2 supercomputer. All seven workstations are connected via a dedicated high speed data communication network (FDDI). These facilities, combined with access to national CRAY supercomputer facilities and the College of Engineering's Computer-Aided Engineering Center provide access to a wide variety of state-of-the-art software tools relevant to the proposed research.